AESF SUR/FIN '88
Technical Conference Proceedings



June 27-30, 1988
Los Angeles Convention Center
Los Angeles, CA

Session B: Research

American Electroplaters and Surface Finishers Society, Inc.
75th Annual Technical Conference - Los Angeles
Research
Session B

Development of Chemical Sensors for Ions in Plating Solutions **B-1**
Robert F. Savinell, Chi-Jin Chen, Sharon Reid and Chung-Chiun Liu
Department of Chemical Engineering
Case Western Reserve University
Cleveland, OH 44106

Selective Pulse Plating of Gold and Tin-Lead Solder **B-2**
D-T. Chin and M.K. Sunkara
Department of Chemical Engineering
Clarkson University
Potsdam, NY 13676

Thickness Effects on the Mechanical Properties of Electrodeposits **B-3**
Ingon Kim and Rolf Weil
Stevens Institute of Technology
Hoboken, NJ 07030

Factors Affecting Low Temperature Interdiffusion **B-4**
L. Giannuzzi, H.W. Pickering and W.R. Bitler
The Pennsylvania State University
University Park, PA 16802

Effects of Additives in Acid Chloride Zinc Deposition **B-5**
T.J. O'Keefe, J.S. Cuzmar and Y.S. Park
Graduate Center for Materials Research
University of Missouri-Rolla
Rolla, MO 65401

S. Wagner
Missouri Electrochem Inc.
10958 Lin-Valle Drive
St. Louis, MO 63123

Addition-Agent Effects in Functional Chromium Deposits **B-6**
N.M. Martyak
M&T Chemicals, Plating Division
Rahway, NJ 07065

R. Weil
Stevens Institute of Technology
Hoboken, NJ 07030

B-1

Research Session B

Development of Chemical Sensors For Ions in Plating Solutions

Robert F. Savinell, Chi-Jin Chen,
Sharon Reid and Chung-Chiun Liu
Department of Chemical Engineering
Case Western Reserve University
Cleveland, OH 44106

DEVELOPMENT OF CHEMICAL SENSORS FOR IONS IN PLATING SOLUTIONS

Robert F. Savinell, Chi–Jin Chen, Sharon Reid, Chung–Chiun Liu
Department of Chemical Engineering
Case Western Reserve University
Cleveland, OH 44106

Summary

Electrochemical sensors fabricated by microelectronic thick and thin film metallization techniques are being developed for detecting ions in plating solutions. The advantage of this approach is that small, reliable and fast responding sensors can be fabricated on a relatively small single substrate. The design of this sensor uses interconnected square element working electrode and band electrode arrays in order to enhance the sensor response time and sensitivity. However, possible interaction and interference of the reactions occuring at electrode surfaces in this design must be considered. This study analyzes the potential interactions and provides a mathematical model of the sensor design. The validity of this mathematical model is verified by experimental investigation for sensing ferric ion in a simulated Zn–Fe plating bath solution. Over the ferric ion concentration range of 1 to 6 gpl, a good linear relation exists between the current output of the sensor and the ferric ion concentration. Both the mathematical model established and the fabrication approach used in this study are potentially important for the development of practical sensors for the plating industry.

Introduction and Background

The plating and surface finishing industry has a need for simple chemical sensors to detect specific ion concentrations. In this research program sponsored by the American Electroplaters and Surface Finishing Society (AESF), we are developing sensor devices for possible applications in the plating industry. In this paper, we will discuss our results to date on developing a sensor for detecting and quantifying ferric ion in Zn–Fe (and Ni–Fe) alloy plating baths. The accumulation of ferric ion in these baths is known to be detrimental to the performance of the bath [1].

Our approach employs electrochemical techniques. Namely, we apply controlled potential amperometry and linear sweep voltammetry using arrays of microelectrodes. Electrochemical techniques are selective in that only certain electrochemical reactions can occur within a properly chosen potential window. In the case of the ferric/ferrous couple, the standard electrode potential of the reaction

$$Fe^{3+} + e \rightleftharpoons Fe^{2+}$$

occurs at 0.55 volts positive of a silver/silver chloride reference electrode. Ignoring concentration effects and using an appropriate electrode material (e.g. platinum), an overpotential of several hundred millivolts negative of the standard electrode potential of the reaction will produce a net cathodic reaction resulting in a current which is proportional to the ferric ion concentration. Interference from zinc, sulfate or chloride ions and dissolved oxygen are expected to be minimal under this condition.

The uniqueness of our approach is that the sensor is fabricated by using microelectronic techniques. In this way an array of microsensors can be placed on a single small size substrate, i.e. a chip. Also with the sensing electrode, the reference and counter electrode can be fabricated onto the same chip. This approach permits the fabrication of a small sensor which will be practical for installation in industrial processes.

There are other advantages using microelectronic techniques to fabricate the sensor. One advantage is that very reproducible electrode surfaces can be produced using photolithographic reduction, and thick or thin film metallization. Therefore, since the current is directly related to the electrode surface area, the calibration of these electrodes will be simplified. Also, small dimensional sensing electrodes are fast responding with enhanced current densities [2,3]. The advantage of having an array of electrodes with proper signal processing is that redundancy of electrodes leads to more reliable measurements.

The geometrical configurations of the sensing electrodes developed are arrays of square electrode elements and band–type electrodes (see Figure 1). In this figure, three electrodes are shown on a single chip. The bottom electrode, counter electrode, represents three band electrodes in parallel. The center electrode is a Ag/AgCl reference electrode. The top electrode, the sensing electrode, is the same as the bottom but strips of insulating epoxy are overlayed perpendicularly to them. This gives an array of square electrode elements which are interconnected in parallel. The width of the band electrode or the size of the square electrode element is the characteristic dimension. The smallness of this dimension is responsible for the microelectrode type performance. The length of the band electrode or the number of elements in an array can be increased to yield larger currents, therefore enhancing the sensitivity of the electrode.

In this paper the testing results of an array of square sensing electrode elements for dectecting ferric ion in Zn–Fe plating baths are reported. Interactions between adjacent electrodes are examined by mathematical simulation of a band electrode configuration. These simulations result can be applied to arrays of square electrode elements. The comparison of simulation results with experimental data is reported.

Modeling the Band Electrode

For a single electrode with micro dimensions, the current density is enhanced significantly due to the effect of radial diffusion. However, different behaviors arise for electrode arrays. At very short time, each electrode acts like an isolated single electrode. However, at a longer time, the electrode arrays will react like an apparent electrode of much larger dimensions (about $1/r$ times a single element, where r is the fraction of conducting area) at which the mass transfer approaches to semi–infinite linear diffusion.

A model which simulates the limiting current response of both single and multiple electrode cases to a step change in potential is developed. This model examines the interactions between the band electrodes and will be useful for designing sensor devices with optimum performance.

According to Fick's law, the corresponding partial differential equation which describes the unsteady, semi–infinite diffusion of uncharged species (or dilute charged species in a supporting electrolyte) to band–shaped multiple electrodes as shown in Fig. 2 is given by:

$$\frac{\partial C}{\partial t} = D \left(\frac{\partial^2 C}{\partial x^2} + \frac{\partial^2 C}{\partial y^2} \right) \tag{1}$$

where C is the concentration of ferric ion and D is the diffusion coefficient.
The initial and boundary conditions are as follows:

$$t = 0, \qquad C = C^o \tag{1.1}$$

$$t > 0,\ x = a/2, \qquad \frac{\partial C}{\partial x} = 0 \tag{1.2}$$

$$t > 0,\ x = 0, \qquad \frac{\partial C}{\partial x} = 0 \tag{1.3}$$

$$t > 0,\ y = 0,\ 0 \le x \le w/2, \qquad C = 0 \tag{1.4}$$

$$t > 0,\ y = 0,\ w/2 < x < (w+a)/2 \qquad \frac{\partial C}{\partial y} = 0 \tag{1.5}$$

$$t > 0,\ y \to \infty, \qquad C = C^o \tag{1.6}$$

The third boundary condition (1.4) states that under the conditions of experiment the concentration of the active species is reduced to zero immediately upon application of the potential step, i.e., the reaction is purely diffusion controlled. Thus the local diffusion limited current density to the system is written as:

$$i(x) = nFD \left(\frac{\partial C(x)}{\partial y} \right) \Big|_{y=0} \tag{2}$$

where n is the number of electrons being transferred and F is Faraday's constant. While the average dimensionless limiting current density, $\bar{i}_{avg}$, is :

$$\bar{i}_{avg} = \int_0^{w/2} \frac{\partial \bar{C}(x)}{\partial y} \Big|_{y=0} dx \tag{3}$$

where $\bar{C}$ is the dimensionless concentration, $\bar{C} = C/C^o$.

Similarly, the diffusion equations for single band–shaped electrode are the same as for multiple ones (Eqns. (1)–(3)); however one boundary condition (Eqn. (1.2)) is substituted by :

$$t > 0,\ x \to \infty, \qquad C = C^o \tag{1.7}$$

The diffusion equation (Eqn. (1)) associated with initial and boundary conditions (Eqns. (1.1)–(1.7)) for both multiple and single electrode cases are solved

by numerical method. The Hopscotch finite difference algorithm proposed and analyzed by Gourlay [4,5] was chosen to accomplish the simulation. This technique is more accurate and faster than conventional explicit methods; yet requires less storage space than implicit methods.

The results of the model predictions and comparison with experimental data are given later in this paper.

Experimental

Fabrication of Electrode Array: The experimental electrode used was a band–type electrode type fabricated by conventional photographic reduction, photolithographic and thick film metallization techniques [6,7]. One inch square alumina substrate having a thickness of 0.025 inch (Coors Industries) was used, and platinum ink(#A4731, Engelhard) was employed for the thick film metallization.

The actual arrangement of the electrodes on the substrate is shown in Figure 1. This arrangement has two sets of electrodes separated by a reference electrode. All three of these electrodes could be used in a self–contained sensor device. In this research, the set of band electrodes and the array of square electrode elements were tested independently against an external counter and reference electrode.

Testing Procedure: A three compartment cell was used to test the array and band electrodes. An external platinum counter electrode and a calomel reference electrode (SCE) were used in this work. A potentiostat (model 273, Princeton Applied Research) was used to apply potential steps and linear potential sweeps and the resulting current/time transients were recorded on an X–Y recorder. In later experiments oxygen was suppressed by sparging the solution with nitrogen prior to measurements and blanketing the solution with nitrogen during the experiment.

Experiments performed to evaluate the array of electrode elements in simulated plating solutions were with the following composition [1]: 55 gpl Na_2SO_4, 153.8 gpl $ZnSO_4$, 3 gpl citric acid, 347.5 gpl $FeSO_4$ and 0–6 gpl ferric ion. The testing of band electrodes to corroborate the modeling simulation was done in a solution of 1M $ZnSO_4$ and 0–6 gpl ferric ion.

Results and Discussion

Evaluation of Electrode Arrays in Simulated Zn–Fe Plating Solutions

A series of tests on the array electrode configuration was performed with varying ferric ion concentration in a simulated plating solution. In these tests the solutions were not deoxygenated. The potential of the working electrode was scanned (10–100mV/s) from +200 mV to –200 mV vs SCE. This represents a potential range where ferric ion should be reduced without interference from other reactions. Two characteristics of the data are noted. First, the hysteresis during the scan appears to increase as the ferric ion concentration increases. Secondly, this hysteresis becomes less at the slower scan rates. The scans with simulated solutions without ferric ion were near the zero current baseline. This indicates that dissolved oxygen does not interfere with sensor sensitivity to ferric ion. The linear response of the sensor is shown in Figure 3.

Model Simulation Results and Experimental Verification

Interactions between elements in band–shaped electrode arrays and their effects on the transient current response to a potential step were investigated using ferric ion reduction. The experimental data from deoxygenated electrolytes are compared with the model predictions. In comparison, the total current from simulation takes into account both contributions of single–electrode and multiple electrodes :

$$I = nFDC^{o}l\left(4(\bar{i}_{avg})_{int} + 2(\bar{i}_{avg})_{ext}\right) \qquad (4)$$

where, $(i_{avg})_{int}$ and $(i_{avg})_{ext}$ represent the dimensionless current density predicted from multiple electrode and single electrode models respectively. Fig. 4 shows excellent agreement between the experimental results at band electrode arrays and those predicted from Eqn. (4). In these comparisons, a diffusion coefficient of $D = 6 \times 10^{-6}$ cm^2/s from literature [8] was used in the calculations.

Two characteristic limiting bounds for electrode arrays are predicted from simulations and found from experimental results with platinum electrodes as shown in Fig. 4. At very short times, when diffusion layer thickness is smaller than the width of each single electrode, the lower bound is formed since the current behaves like semi–infinite linear diffusion to each electrode. The lower bound is given by the Cottrell equation [9] and rewritten in dimensionless form :

$$(\bar{i}_{avg})_{low} = \frac{Nw}{\sqrt{\pi Dt}} \qquad (5)$$

where N is the number of electrodes having width ,w.

As time increases, the diffusion layer thickness of each electrode increases gradually, and finally the diffusion layer overlaps adjacent electrodes. The array of single electrodes now form an apparent planar electrode which is large enough such that the edge effect is negligible. Therefore, the current behavior approaches an upper bound as semi–infinite diffusion to an apparent planar electrode, namely:

$$(\bar{i}_{avg})_{up} = \frac{Nw(2/r+1)}{\sqrt{\pi Dt}} \qquad (6)$$

The current–time relationship of experimental data is well confined within two limiting bounds (Eqn. (5) and Eqn. (6)) as shown in Fig. 5. Again, as shown, the model predictions are confirmed with experimental data.

Conclusions

Based on the results to date, the following conclusions can be formulated:

1. An array of miniature electrodes were tested in a simulated Zn–Fe plating solution. The electrodes responded to a linear potential sweep with limiting currents directly proportional to the concentration of ferric ion. Oxygen reduction did not interfere in the test.

2. The current transient to a potential step predicted by a mathematical model was shown to be bounded by semi–infinite linear diffusion models (at the low end by the single electrode result, and at the high end by an apparent electrode dimension).

3. Experimental data was in excellent agreement with the model predictions.

4. The research indicates that this approach will yield reliable and fast responding sensors for detecting ferric ions in plating solutions.

Acknowledgement

This research is supported by an AESF Fellowship (Project #73 of the Research Board) and by the National Science Foundation (CBT–869073).

References

1. AES Fourth Continuous Strip Plating Symposium, Proceedings of the Symposium held at the Continental Hotel, Chicago, IL, May 1–3, 1984 (American Electroplaters society, Florida), 1984.

2. P.M. Kovach, W.L. Caudill, D.G. Peters and R.M. Wightman, J. Electroanal. Chem., 185, 285(1985).

3. C.A. Amator, M.R. Deakin and R.M. Wightman, J. Electroanal. Chem., 206, 23(1986).

4. D. Shoup and A. Szabo, J. Electroanal. Chem., 160 (1984) 1.

5. A.R. Gourlay, J. Inst. Math. Appl., 6 (1970) 375.

6. C.C. Liu, M.R. Neuman, K.L. Montana, and M.C. Oberdoerster, Marine Technol., 16 (1980) 468–472.

7. C.C. Liu and M.R. Neuman, Diabetes Care, 5 (1982)275–279.

8. D.J. Pickett, "Electrochemical Reactor Design," Elsevier, (1979) p.99

9. F.G. Cottrell, Z. Phys. Chem., 42 (1902) 385.

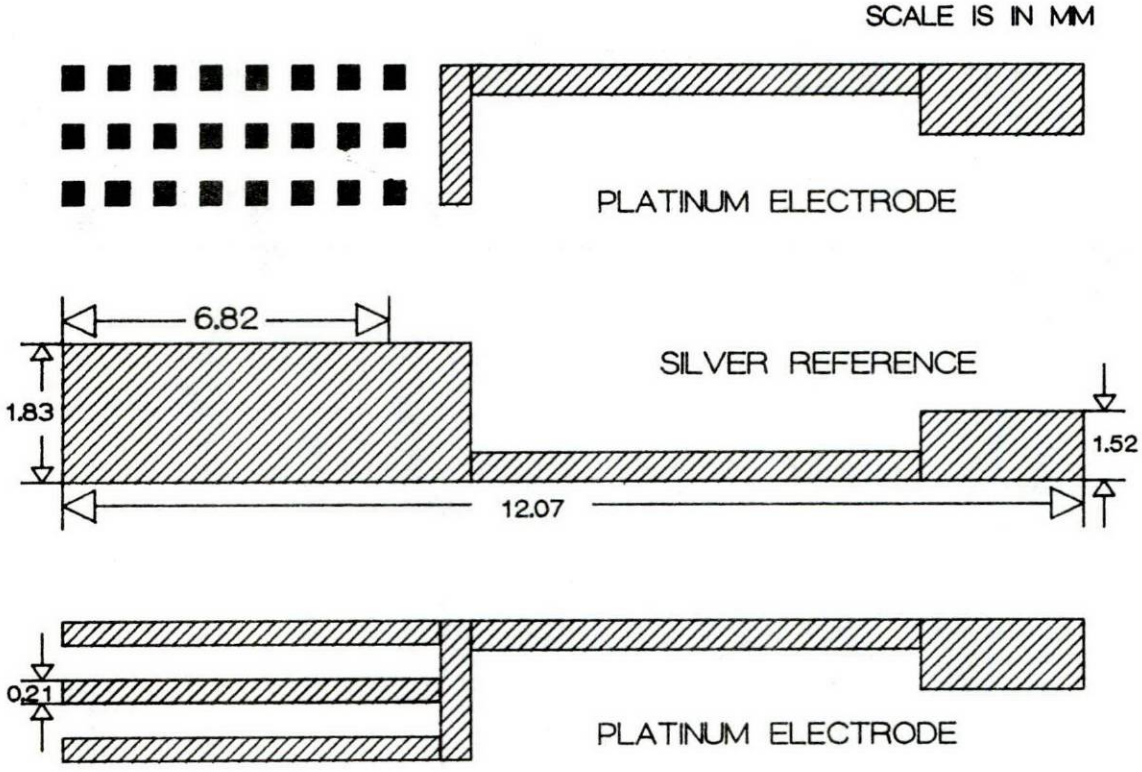

Fig. 1 Schematic of Three-Electrode Micro-Sensor Fabricated at CWRU

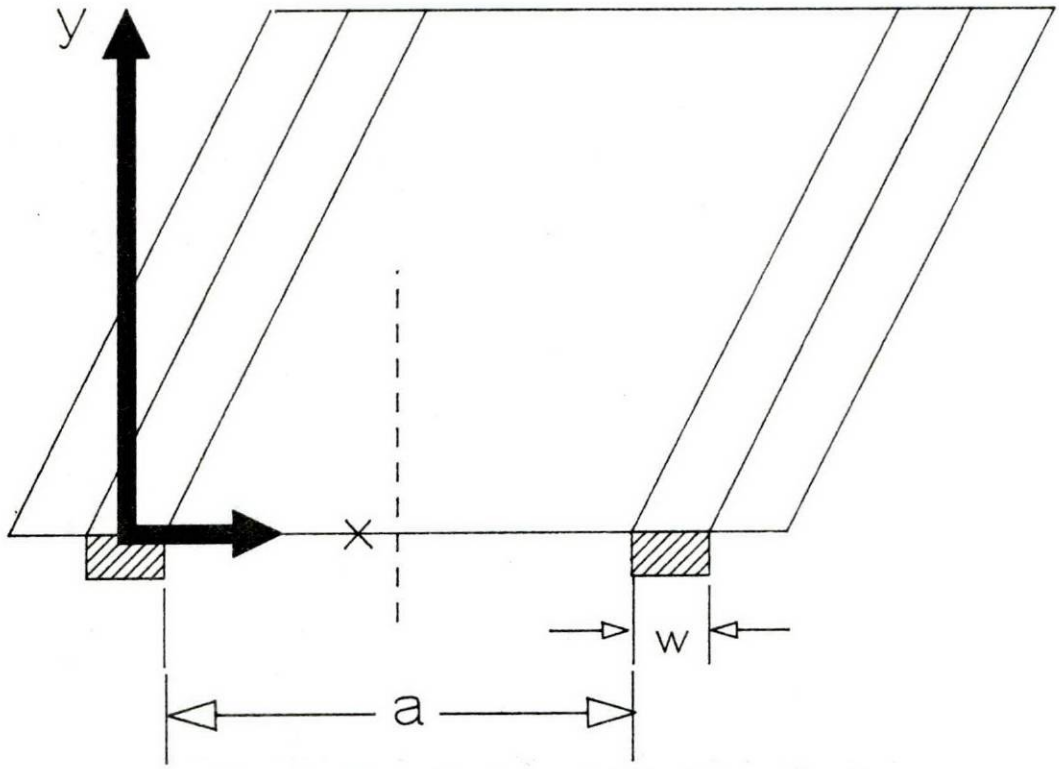

Fig. 2 Coordinate of Modeling System

W:electrode width ; a:the distance between two electrodes

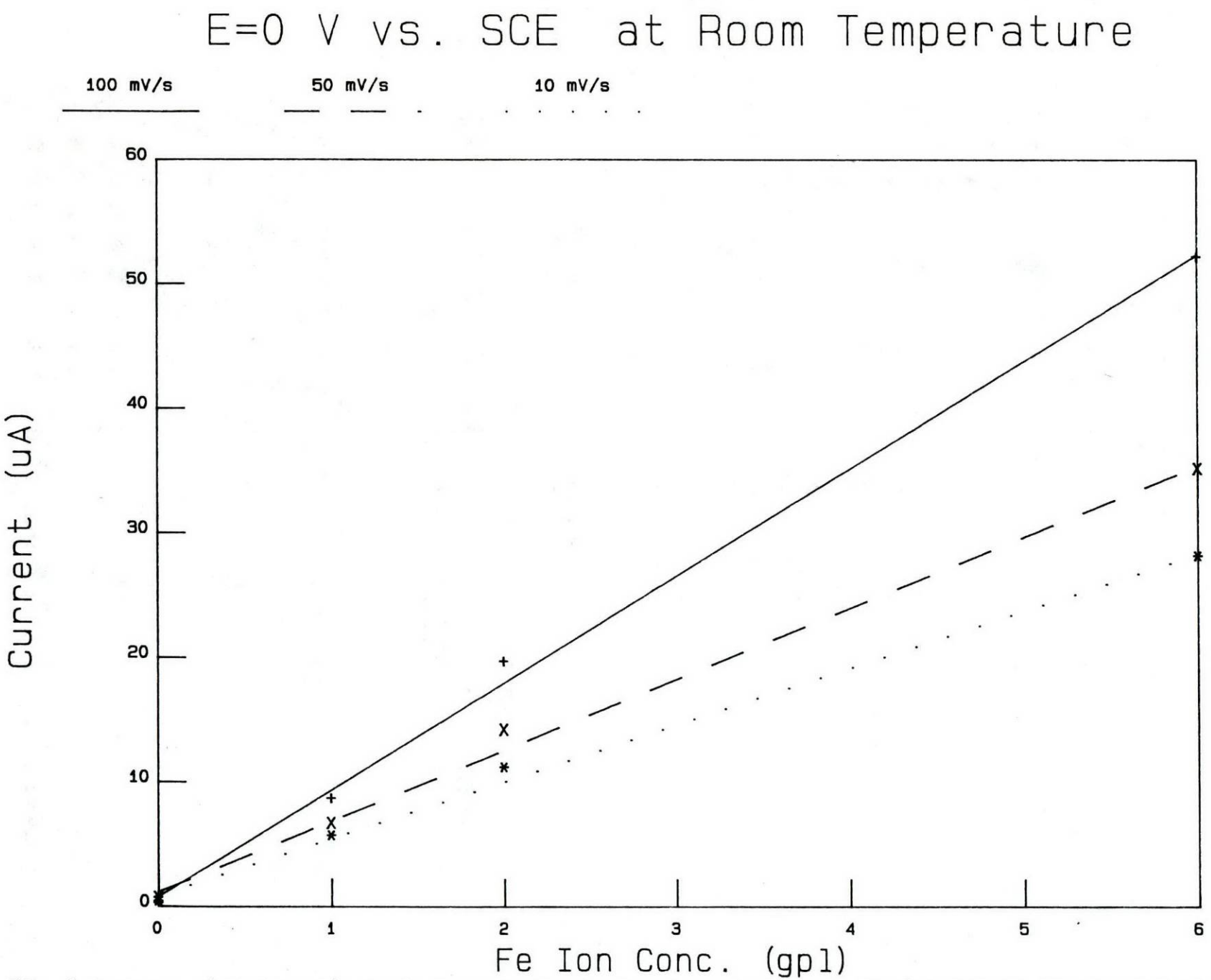

Fig. 3 Response of Working Electrode Array to Ferric Ion Concentration in Simulated Zn-Fe Plating Solution.

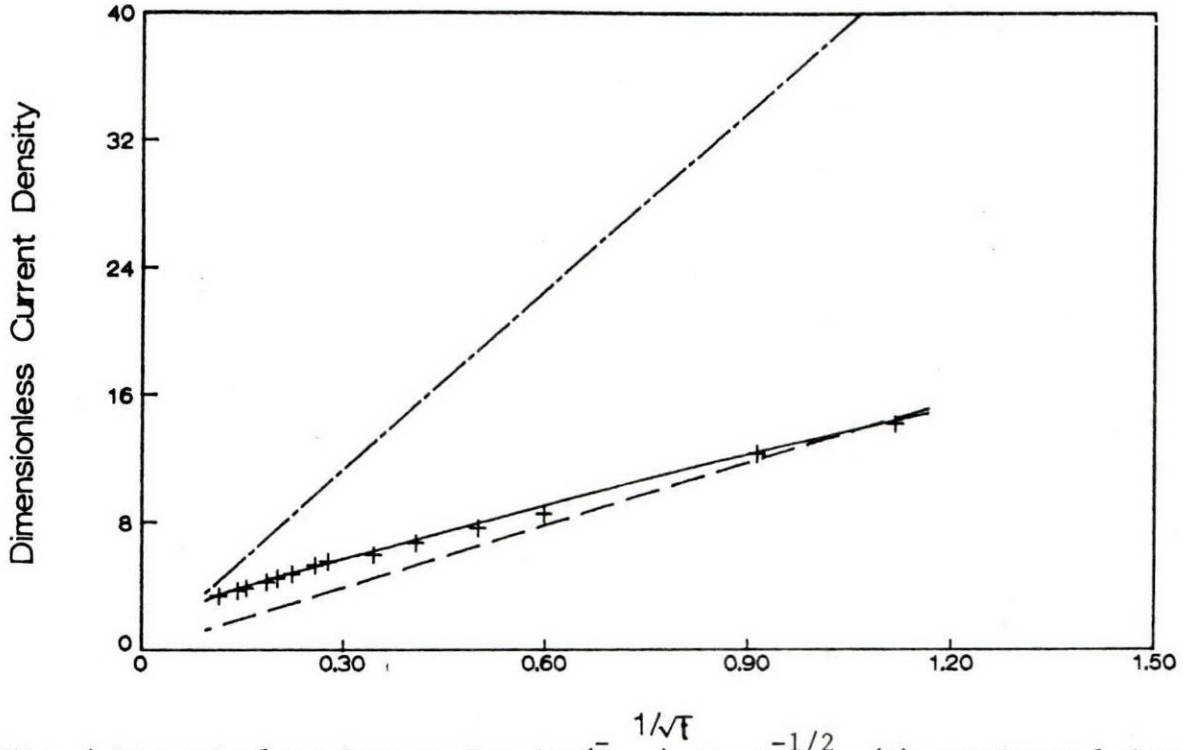

Fig. 4 Dimensionless Current Density($\bar{i}_{avg}$) vs. $t^{-1/2}$. (+)experimental data; (——)model prediction; (---)lower bound(from eqn.(5)); (—·—)upper bound(from eqn.(6)). Experimental condition : $Fe_2(SO_4)_3$ 36mM; $ZnSO_4$ 1M. Applied potential -0.25V.

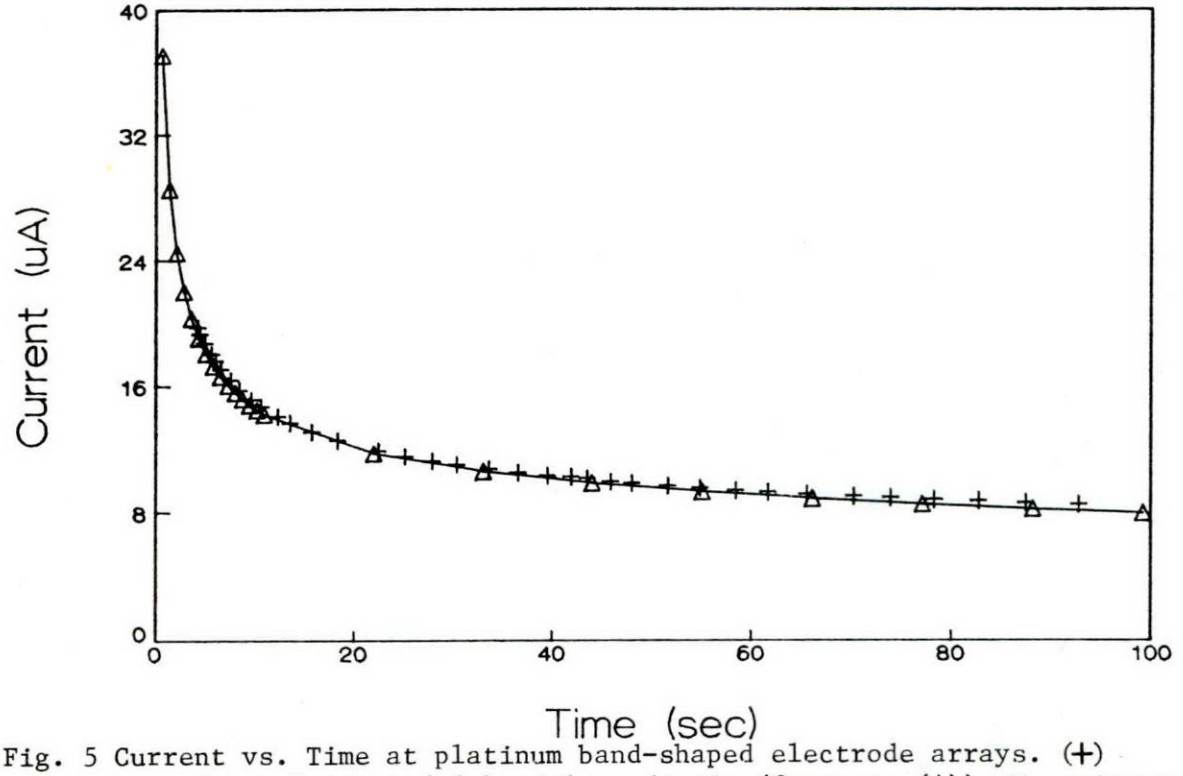

Fig. 5 Current vs. Time at platinum band-shaped electrode arrays. (+) experimental data; (—△—)model prediction(from eqn.(4)). Experimental condition : $Fe_2(SO_4)_3$ 5mM; $ZnSO_4$ 1M. Applied potential -0.25V.

B-2

Research Session B

Selective Pulse Plating of Gold and Tin-Lead Solder

D-T. Chin and M.K. Sunkara
Department of Chemical Engineering
Clarkson University
Potsdam, NY 13676

SELECTIVE PULSE PLATING OF GOLD AND TIN-LEAD SOLDER

D-T. Chin and M.K. Sunkara
Department of Chemical Engineering
Clarkson University
Potsdam, New York 13676

ABSTRACT

This study is concerned with the use of pulse current to selectively deposit metal on a localized area of an unmasked cathode. The localization of electrodeposition is achieved by directing a small anode toward a large maskless cathode at the desired location, and by applying high peak pulse current density of 1-20 A/cm^2. In this paper, the experimental results obtained with a 24 Kt hard acid bright gold bath and a 60% tin - 40% lead solder bath are presented. The effect of current pulse on the metal distribution and morphology of electrodeposits is discussed.

INTRODUCTION

Selective plating (also called spot plating) has received increasing attention in the metal finishing industry because of the high cost of noble metals and the need to localize metal deposition in the manufacture of electronic contacts and printed circuit boards. The localization of metal deposits is generally achieved by the application of cathode masks, photo-resist coatings, and brush platings. These techniques require a series of pre-plating and post-plating treatment procedures, rendering high production cost in the overall finishing process.

The purpose of this work is to study the feasibility of using pulse plating to localize the electrodeposition process on a maskless cathode. Several theoretical inveatigations (1,2) have shown that in pulse plating with short pulse durations and high pulse frequencies, very high instantaneous pulse current densities on the order of 10-100 A/cm^2 can be used without depleting the concentration of metal ions at the cathode surface. At high plating current densities, the primary current distribution prevails, and the throwing power is worse than that of the secondary current distributions. This suggests that spot plating can be achieved by: i) directing a small insoluble anode toward a large unmasked cathode; ii) keeping the anode-cathode spacing at a small value; and iii) applying a high peak pulse current density to localize the electrodeposition at the selected area facing the anode.

This paper describes an experimental study of the effect of pulse current density, duty cycle, pulse period, and anode-cathode spacing on the metal distribution and morphology of gold, and 60% tin - 40% lead solder deposits on a maskless cathode. The results of pulse plating are compared to those of DC plating at the same average current density. The current distribution on the maskless cathode was calculated with a two dimensional mathematical model.

EXPERIMENTAL

The details of experimental setup and instrumentation have been described in previous publications (3,4). The electroplating cell consisted of a large unmasked cathode and a small insoluble circular anode. The cathode was supported vertically in the cell, and the circular anode having its exposed plane parallel to that of the cathode was introduced from one side of the cell. The anode-cathode spacing could be adjusted by sliding the anode support rod through a water-tight fitting on the cell wall. A saturated calomel electrode located in a Luggin capillary was used as the reference electrode, and a thermometer inserted through the cell cover was used to measure the electrolyte temperature.

The pulse plating experiments were carried out under the galvanostatic controlled conditions. A function generator (Hewlett-Packard 3311A) connected to a mini-pulsir (LWD Scientific) and a variable resistor was used to generate a rectangular pulsating voltage signal of desired magnitude, duty cycle, and frequency. The pulsating voltage signal was fed to a high power potentiostat (Wenking HP72) and was converted to pulsating current by operating the potentiostat on the galvanostatic mode. A Commodore PET 4032 computer was used to interface with a Hewlett-Packard 3421A digital data acquisition unit to monitor the time-averaged DC plating current, average potential drop between the cathode and reference electrode, and average anode-cathode cell voltage. Suitable software using IEEE 488 interfaces was developed to process the plating data.

The pulse plating of gold was carried out with a 24-Kt acid hard bright gold bath (Orosene 999, Technic Inc.) containing 0.029 M potassium gold cyanide, 0.37 M mono-potassium phosphate, and 0.84 M citrate in the form of citric acid and potassium citrate (pH 4.5). The minor additives in the bath included cobalt chelates and wetting agents. A copper plate, 5 cm long by 5 cm wide by 0.038 cm thick was used as the cathode. A stainless steel disk of 6 mm in diameter flush-mounted on a Teflon sleeve was used as the anode. For each run, the copper cathode was polished with 0.3 micron alumina polishing compound, degreased with methanol, and rinsed in water. It was plated with 0.75 micron bright nickel and then pre-coated with 0.025 micron gold from an alkaline gold strike bath. Pulse plating experiments were carried out over a range of peak pulse current densities 0.025-20 A/cm^2, duty cycles 1-100%, and pulse periods 1-100 ms. Each experiment was terminated after 25 coulombs of charge (based on the time-averaged DC current) had passed through the cell. The metal distribution of gold deposit at the cathode was measured with a coulometric thickness gage (UPA Technology, Inc., Model CM-100), and the morphology of gold deposits was examined under a scanning electron microscope.

The pulse plating of 60% tin - 40% lead solder was carried out using a nonfluoborate bath (Techni-Solder NF acid, Technic Inc.) and a fluoborate bath (Techni-Solder 60/40 Plating Solution, Technic Inc.). The nonfluoborate bath was composed of 0.17 M stannous methyl sulfonate, 0.048 M lead methyl sulfonate, and 15% by volume of methyl sulfonic acid. The

fluoborate bath contained 0.13 M stannous fluoborate, 0.048 M lead fluoborate, and 40% by volume of fluoboric acid. A circular stainless steel disk of 6 mm in diameter was used as the anode, and a large uncoated brass sheet was used as the cathode. For each run, the brass cathode was polished to 0.3 micron smoothness; degreased in methanol; dipped in dilute HCl; and rinsed in water prior to transferring to the cell. The plating experiments were carried out for a range of peak pulse current densities 0.025-10 A/cm^2, duty cycles 1-100%, and pulse periods of 1-1000 ms. The deposit thickness was measured with a coulometric thickness gage (Couloderm CM100, UPA Technology, Inc.), which had been calibrated with a standard coating of 60% tin - 40% lead alloy. It was assumed that the deposit composition did not vary with the plating conditions and with the locations on the cathode substrate.

RESULTS AND DISCUSSION

With the present cell geometry, the active area on the cathode where the electrodeposition took place varied with experimental conditions. Unless otherwise noted, the current density values reported in this section will be all based on the constant anode area. An anode-cathode spacing of 3 mm was used in the plating experiments. All measurements were made at a constant room temperature of 21°C.

(1) Gold Plating

Figure 1 shows the results of metal distribution for DC plating of gold over a range of current densities from 0.025 to 0.2 A/cm^2. The local metal thickness is plotted as a function of radial distance from the center of gold deposit. The gold deposit was thickest at the center and became thinner with increasing radial position. With increasing DC current densities, the thickness at the center decreased, and the metal distribution became less uniform.

The effect of pulse current on the metal distribution of gold is shown in Figure 2. In these runs, the average current density and pulse period were kept at 0.05 A/cm^2 and 10 ms, respectively; whereas the duty cycle varied from 100% (DC) to 1%, corresponding to a range of peak pulse current densities of 0.05-5 A/cm^2. Pulse current increased the thickness of gold deposit at the central area facing the anode, and made the metal distribution more localized than that of DC plating. At 1% duty cycle, the gold deposit at the center was 6 times thicker than that of DC plating.

Figure 3 shows the effect of average current density in pulse plating on the metal distribution of gold deposit. These data were obtained at 10 ms pulse period and 10% duty cycle; the average current density varied from 0.025 to 0.2 A/cm^2, corresponding to a range of peak pulse current density of 0.25-2 A/cm^2. The results were similar to those of DC plating that

increasing average current density increased the localization of gold deposit. The metal thickness at the center with 0.2 A/cm^2 average current density was 3.5 times greater than that obtained with 0.025 A/cm^2.

The effect of pulse period (or frequency) on the metal distribution of gold deposit is shown in Fig. 4; these data were obtained by keeping the average current density at 0.05 A/cm^2 and duty cycle at 10%. A uniform metal distribution was obtained with the pulse plating at 1 ms pulse period (corresponding to 1000 Hz pulse frequency). The metal distribution became less uniform with increasing pulse period (or decreasing pulse frequency). The most localized gold deposit was obtained at 200 ms pulse period (or 5 Hz pulse frequency) as shown in the figure.

The morphology of gold deposit at the central area facing the anode was examined with a scanning electron microscope (SEM). Figure 5 shows a set of photomicrographs obtained with DC plating (Fig. 5a) and pulse plating at 10% duty cycle and 10 ms pulse period (Fig. 5b); the deposits were obtained at the same average current density of 0.05 A/cm^2. The gold deposits exhibited hemispherical nodular growth. The grain size obtained with DC plating was 1-2 microns in diameter. With pulse plating at the same average current density, the grain size increased to 10-15 microns in diameter as shown in Fig. 5. Figure 6 shows the effect of average current density on the morphology of gold deposits with pulse plating at 10% duty cycle and 50 ms pulse period. Increasing the average current density from 0.05 A/cm^2 to 0.2 A/cm^2 caused a decrease in the grain size from more than 10 microns in diameter to 1-2 microns.

(2) 60% Tin - 40% Lead Solder Plating

Figure 7 shows the typical pulse plating results obtained with the nonfluoborate bath at an anode-cathode spacing of 3 mm. In these runs, the average current density and pulse period was kept at 0.1 A/cm^2 and 10 ms, respectively, while the duty cycle changed from 100% (DC) to 1%. This covered a range of peak pulse current densities of 0.1-10 A/cm^2. The pulse current improved the localization of the tin-lead deposition. The thickness of the tin-lead deposit at the center with pulse plating of 1% duty cycle was 6.5 times greater than that of DC plating. The effect of average current density on the tin-lead solder plating was similar to that of copper and gold plating that the metal distribution became more localized with increasing average current densities for a given duty cycle and pulse period.

The metal distributions of tin-lead solder from the fluoborate bath are plotted in Fig. 8 for pulse plating at 0.025 mA/cm^2 average current density and 10 ms pulse period. Uniform metal distribution was obtained with DC plating as shown by the 100% duty cycle curve. Decreasing the duty cycle resulted in increasing localization of the tin-lead solder deposit.

With 1% duty cycle pulse plating, the metal thickness at the center facing the anode was 13 times greater than that of DC plating. Figure 9 shows the effect of pulse periods (or pulse frequencies) on the metal distribution of tin-lead solder from the fluoborate bath. The data in the figure were taken by varying the pulse period from 1 to 1000 ms while keeping the average current density at 0.025 A/cm^2 and duty cycle at 10%. The metal distribution of the tin-lead solder deposits became more localized with increasing pulse period (or decreasing pulse frequency). With 1000 ms pulse period, the deposit at the center was nearly 4 times thicker than that with 1 ms pulse period.

(3) Mathematical Modeling of Current Distribution

The present experimental results may be interpreted with a two dimensional mathematical model for the current distribution on an unmasked cathode. Figure 10 shows the schematic representation of an electrochemical cell used for the theoretical analysis. The cell consists of an infinitely long cathode and a parallel finite anode. The anode has a width of $2L_a$; its exposed surface is flush with a semi-infinte insulation surface as shown in the figure. The center of the cathode is taken as the origin of a pair of rectangular coordinates, x and y, with x being the surface distance on the cathode and y being the vertical distance from the cathode surface. The anode-cathode spacing is H. To simplify the analysis, the following assumptions are incorporated into the model: i) the anode polarization is negligible; ii) the solution is well stirred and the concentration polarization is negligible; iii) the pulse period is sufficiently large (or the pulse frequency is sufficiently low) such that the effect of electric double layer on the current distribution is negligible; and iv) the solution properties, such as conductivity and density, are constant. The anode surface is taken as the reference plane where the solution potential is set to be zero. Accordingly, the governing equations describing the current distribution in the cell may be given by the following equations:

i) Voltage Balance

$$E = E_o + \eta_c + \eta_{ohm} \tag{1}$$

where E is the cell voltage during the plating; E_o is the open-circuit cell voltage; η_c is the local activation overpotential at the cathode; and η_{ohm} is the local ohmic potential drop across the electrolyte between the anode and cathode.

ii) Charge Balance

$$\int_{-\infty}^{\infty} i_c(x)dx + \int_{-L_a}^{L_a} i_a(x)dx = 0 \tag{2}$$

where i_a and i_c are the local current density at the anode and cathode surfaces, respectively. Using the present convention, the cathode current is taken to be negative. Equation (2) states that the total current flowing across the cathode/electrolyte interface must be equal to the total current flowing across the anode/electrolyte interface.

iii) Ohmic Drop in the Cell - The ohmic potential drop, η_{ohm}, in the cell is obtained by solving the two dimensional Laplace equation for the potential distribution in the electrolyte.

$$\frac{\partial^2\phi}{\partial x^2} + \frac{\partial^2\phi}{\partial y^2} = 0 \qquad (3)$$

where ϕ is the electric potential in the solution phase. The associated boundary conditions are:

at the cathode ($y = 0$), $\partial\phi/\partial y = -i_c(x)/k$ (3a)

at the anode ($y = H$, $-L_a \leq x \leq L_a$), $\phi = 0$ (3b)

at the anode insulation plane ($y = H$, $|x| > L_a$),

$\partial\phi/\partial y = 0$ (3c)

at the center line ($x = 0$), $\partial\phi/\partial x = 0$ (3d)

at the edge of the cell ($|x| = \infty$), $\partial\phi/\partial x = 0$ (3e)

where k is the conductivity of the electrolyte.

iv) Activation Overpotential at the Cathode - For a given average current density, the activation overpotential during the pulse plating is different from that of DC plating (1). To simplify the analysis, we choose a semi-empirical approach, i.e., the current density vs. activation overpotential relation will be supplied from a set of empirical polarization data in the form:

$$i_c = f[\eta_c, T, \theta] \qquad (4)$$

where i_c and η_c denote the time-averaged current density and activation overpotential at the cathode; T is the pulse period; and θ is the duty cycle. For a given electrolyte system and pulse current of fixed duty cycle and pulse period, the function 'f' is determined from the experimental polarization measurements (3,4).

Equations (1) - (4) must be simultaneously solved to determine the cathodic and anodic current distributions in the cell. A computer code using Fortran 77 and a finite element technique has been developed to perform the numerical calculations. Figures 11 and 12 show the cathodic and

using Fortran 77 and a finite element technique has been developed to perform the numerical calculations. Figures 11 and 12 show the cathodic and anodic primary current distributions for gold plating from the acid hard gold 0bath. A measured conductivity value of 0.0065 $ohm^{-1}cm^{-1}$ was used for the calculation. The horizontal axis in the figures is a dimensionless distance defined as the ratio of cathode surface distance to half-anode width, x/L_a. The dimensionless anode-cathode spacing, $H^*=H/L_a$, was equal to one. The theoretical current distribution curves at the cathode (Fig. 11) exhibited the same trend as those of experimental metal distribution curves shown in Figs. 1-3. Increasing the average current densities at the anode improved the localization of metal deposition at the cathode. The agreement between the theory and experiments was reasonably good for both the DC and pulse platings. The theory also reveals that the current distribution at the anode is not uniform. The local anodic current density is high near the edge of the anode, and decreases toward the center. The anodic current distribution becomes less uniform with increasing average anode current densities as shown in Fig. 12.

CONCLUSIONS

A study has been made of the selective pulse plating of gold and 60% tin - 40% lead solder on localized areas of an unmasked cathode. The localized deposition was achieved by directing a small anode toward the unmasked cathode at a small anode-cathode spacing, and by applying a high pulse current density. The results indicate that the metal distribution at the cathode became more localized with increasing peak pulse current density, with decreasing duty cycle, and with increasing pulse period (or decreasing pulse frequency). Highly localized gold and tin-lead solder deposits were obtained by operating the pulse plating at: i) the anode-cathode spacing less than half anode diameter (or width); ii) small duty cycles less than 1-10%; iii) high instantaneous pulse current densities greater than 1-10 A/cm^2; and iv) high pulse period of 0.05-1 s (or 1-20 Hz). Pulse current also changed the morphology of gold deposit. At the same average current densities, the individual grains of gold deposits obtained with pulse plating were much larger than those obtained with DC plating. For a given pulse period and duty cycle, the size of gold grains decreased with increasing average current densities. The experimental results were interpreted with a two dimensional mathematical model for current distribution in the plating cell. The calculated cathodic current distribution for gold plating agree qualitatively with experimental metal distribution curves.

ACKNOWLEDGEMENT

The authors gratefully acknowledge the financial support of AESF. Thanks are also due to James Voytko of Sandia National Laboratories for his encouragement and many helpful discussions.

REFERENCES

1. D-T. Chin, J. Electrochem. Soc., 130 1657 (1983).

2. N. Ibl, Proc. AESF 2nd Int'l Pulse Plating Symp. (1981).

3. D-T. Chin and N.R.K. Vilambi, 73rd AESF Annual Technical Conference Proceedings, paper G5 (1986).

4. N.R.K. Vilambi and D-T. Chin, Plating and Surface Finishing, 75, No. 1, 67 (1988).

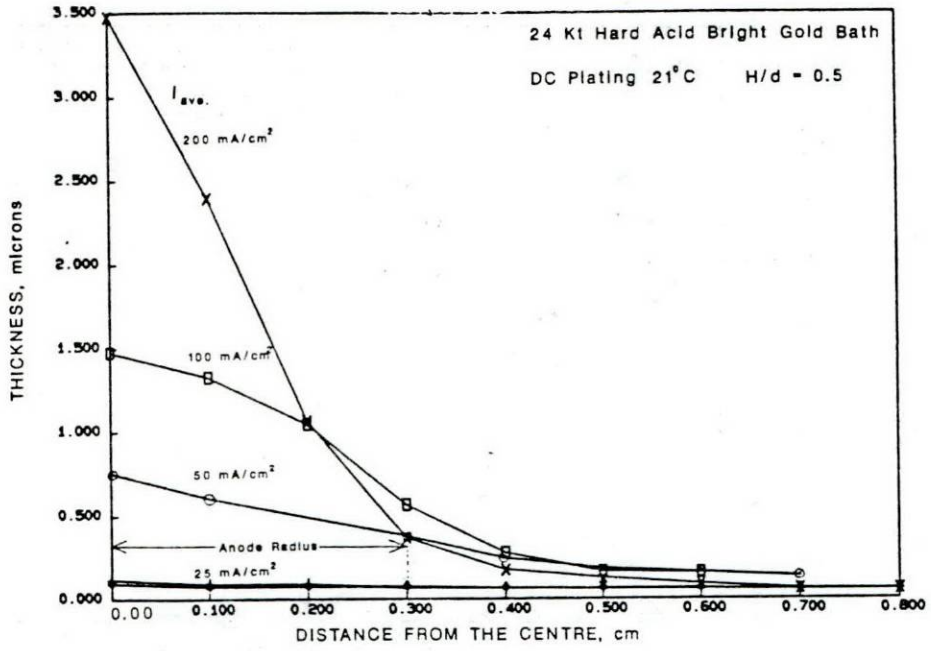

Figure 1. Thickness distribution of gold deposits with DC plating.

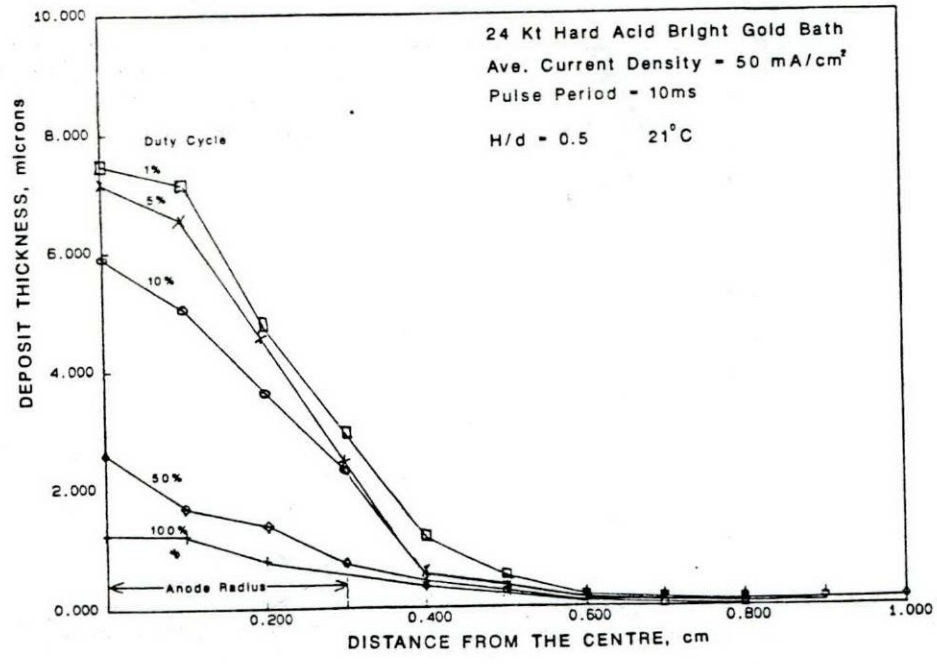

Figure 2. Thickness distribution of gold deposits with pulse plating.

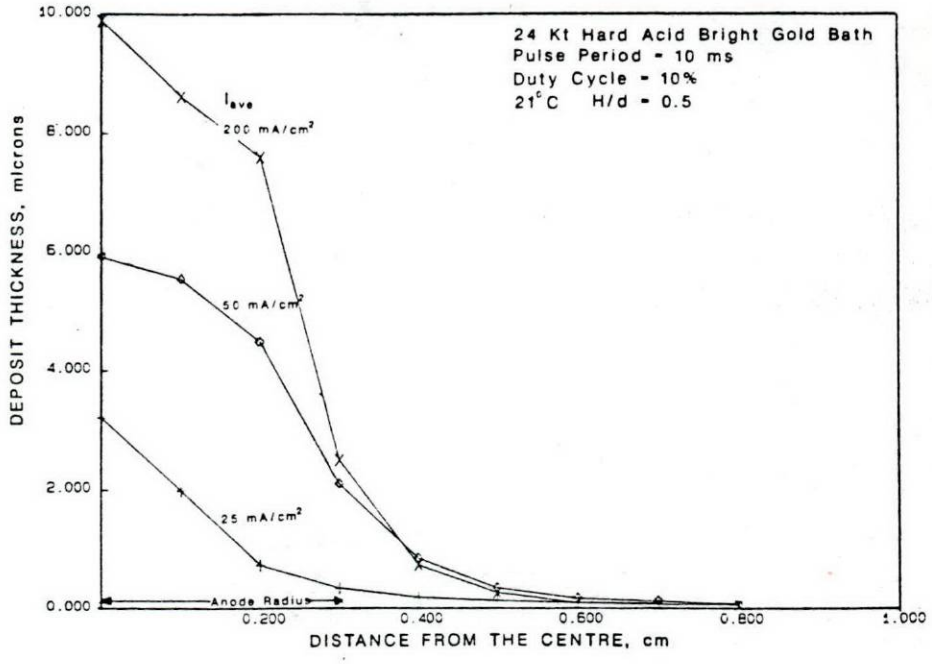

Figure 3. Effect of average current density on the metal distribution of gold deposits in pulse plating.

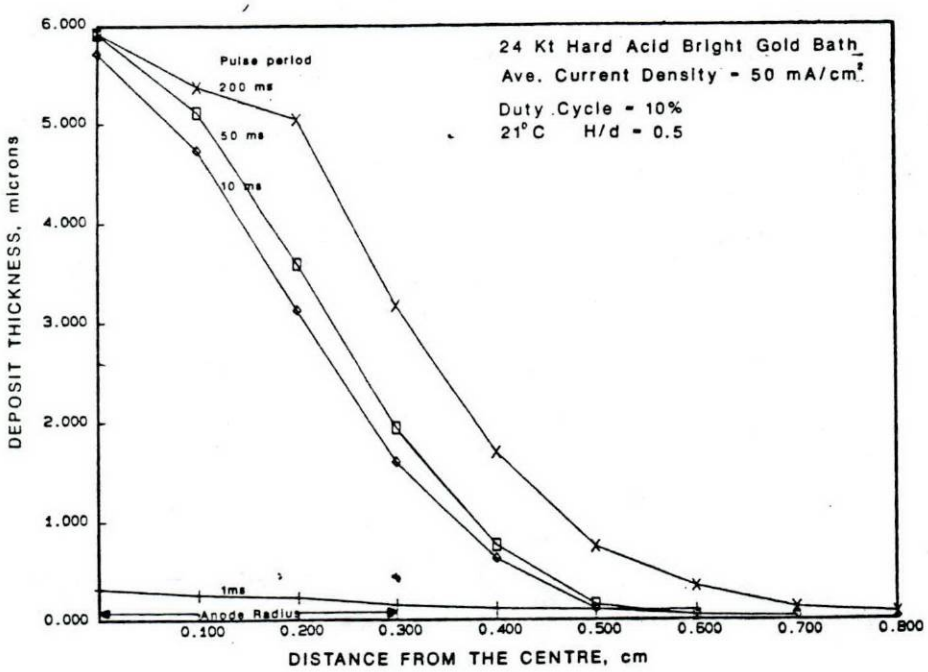

Figure 4. Effect of pulse period on the metal distribution of gold deposits in pulse plating.

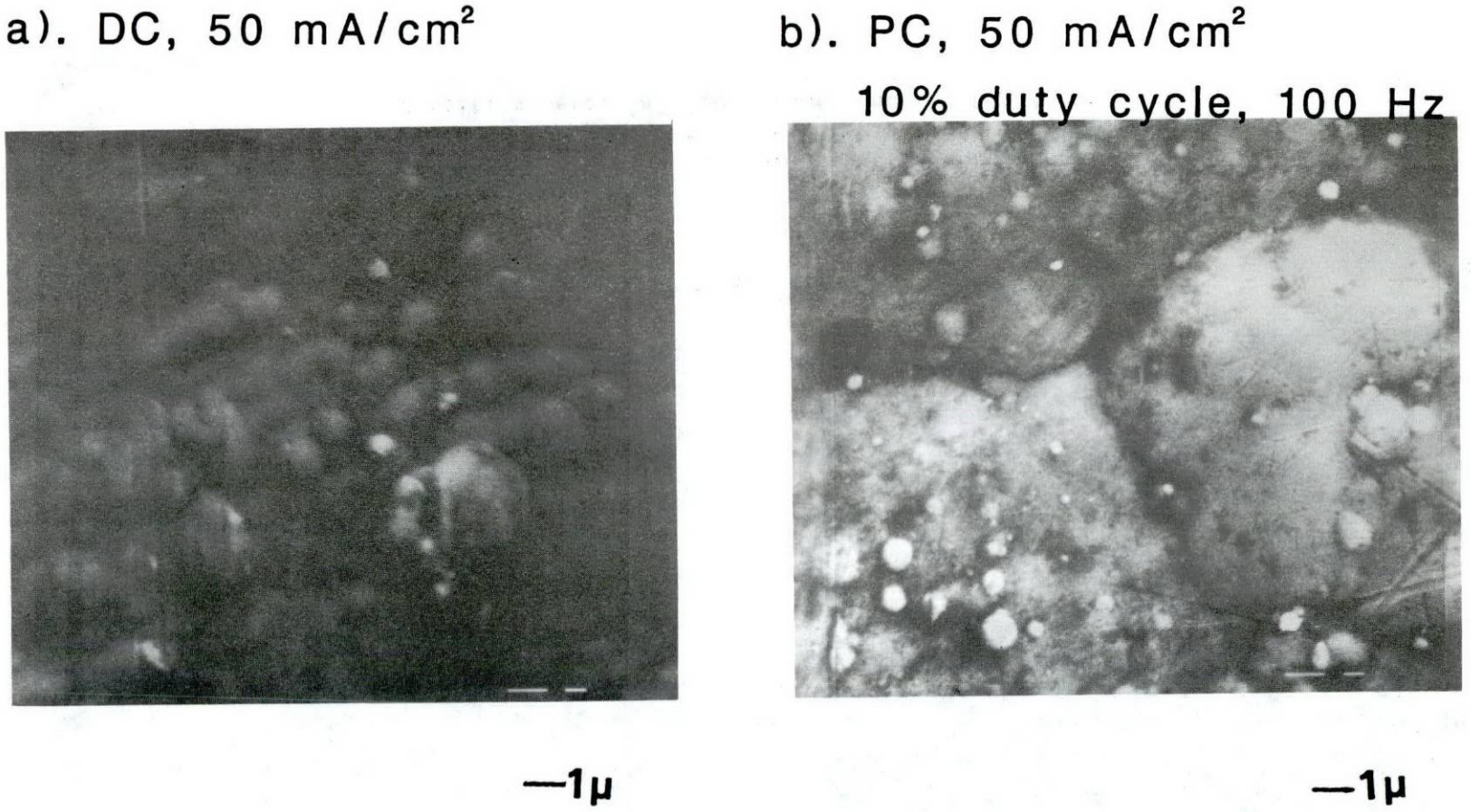

Figure 5. SEM photomicrographs of gold deposits obtained with: (a) DC plating; and (b) pulse plating at 10% duty cycle and 10 ms pulse period. The average plating current density for the both deposits was 0.05 A/cm^2.

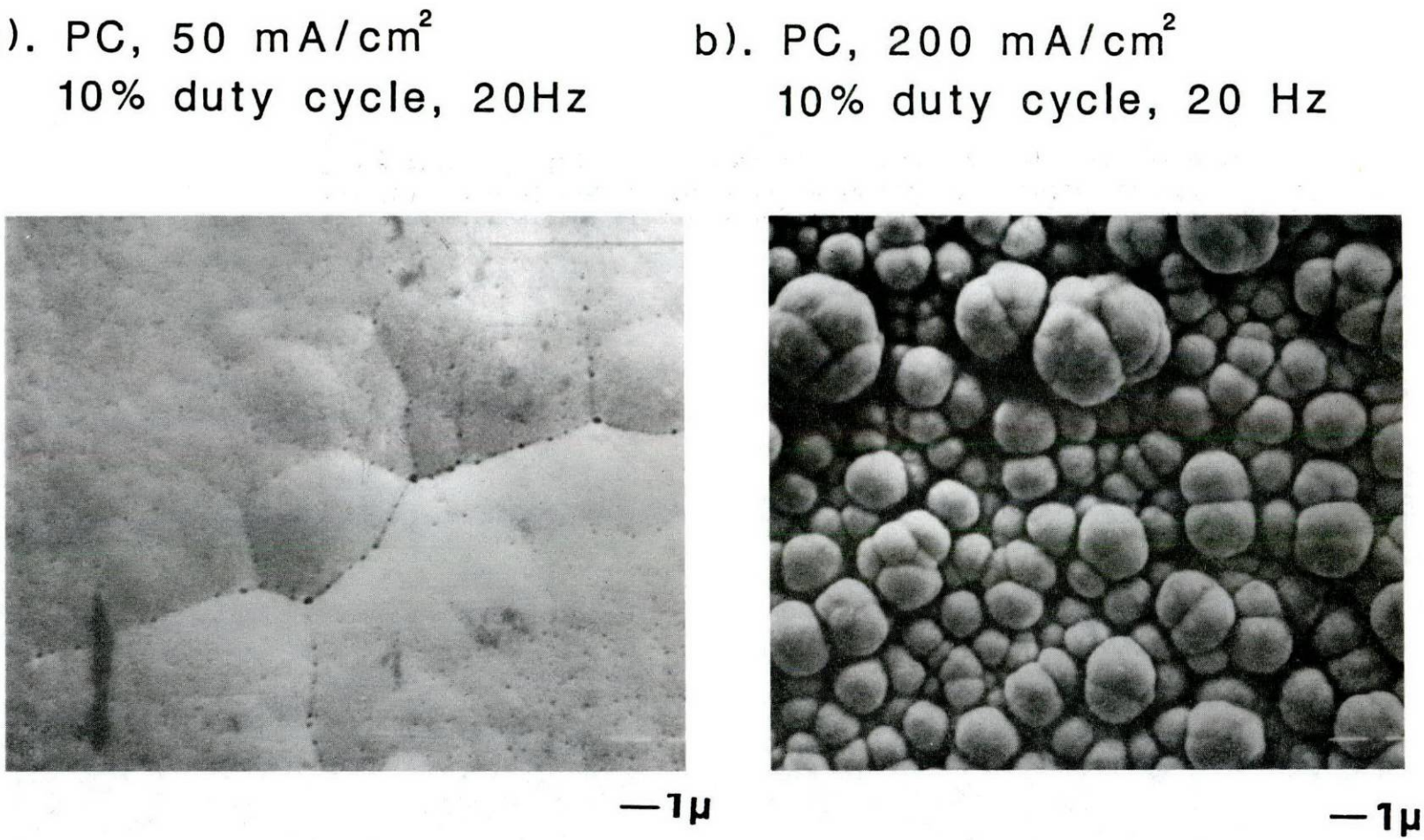

Figure 6. SEM photomicrographs of gold deposits obtained with pulse plating at 10% duty cycle and 50 ms pulse period. The average current densities were: (a) 0.05 A/cm^2; and (b) 0.2 A/cm^2.

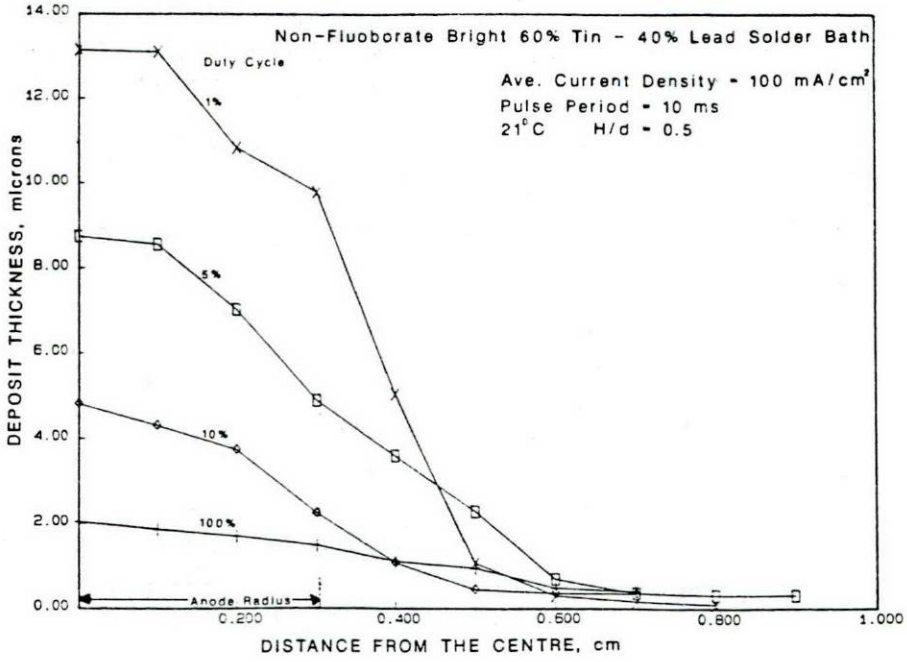

Figure 7. Thickness distribution of tin-lead solder deposits obtained with pulse plating from the nonfluoborate bath.

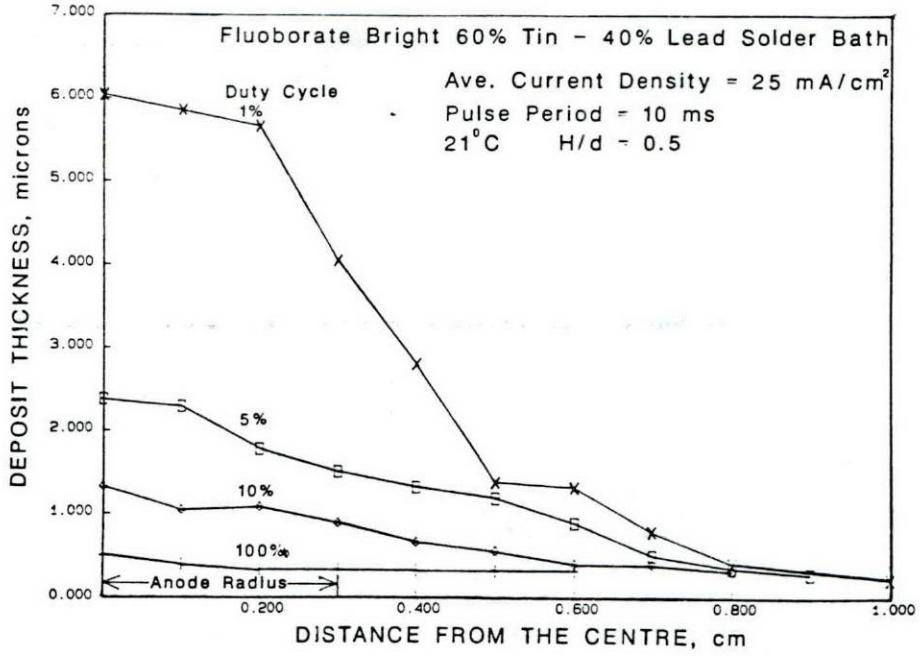

Figure 8. Thickness distribution of tin-lead solder deposits obtained with pulse plating from the fluoborate bath.

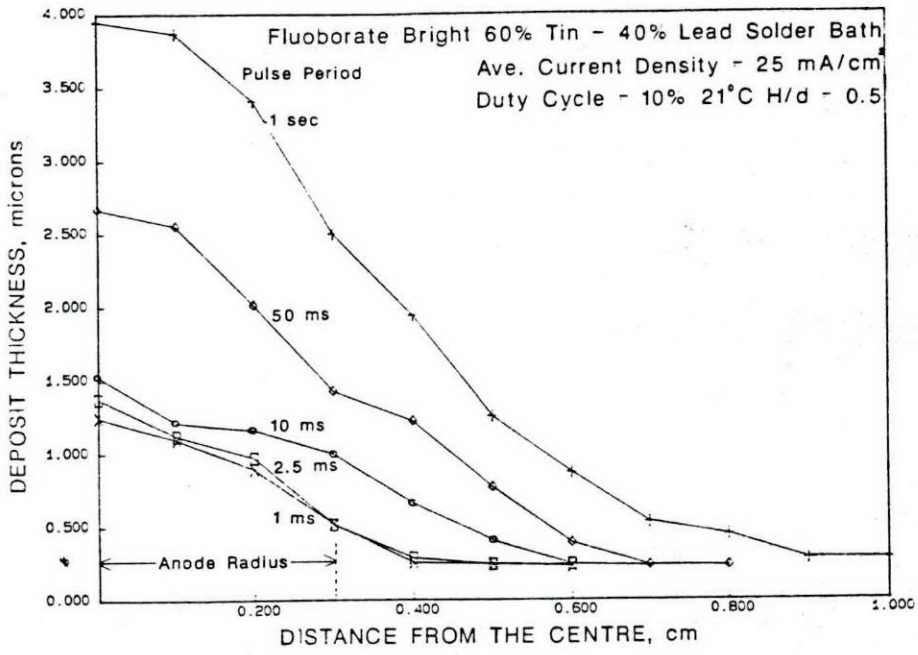

Figure 9. Effect of pulse period on the metal distribution of tin-lead solder deposits from the fluoborate bath.

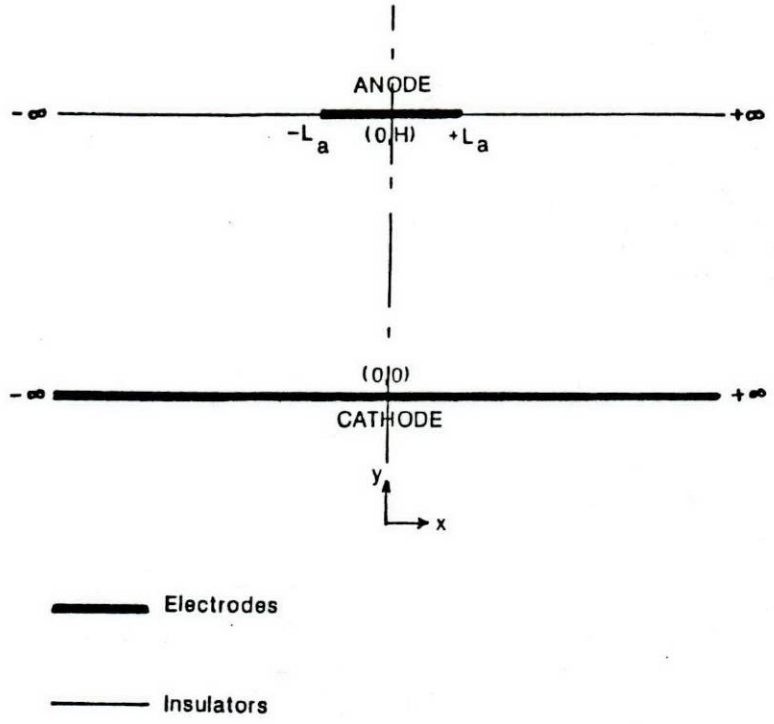

Figure 10. Schematic diagram of electrode geometry used in mathematical modeling.

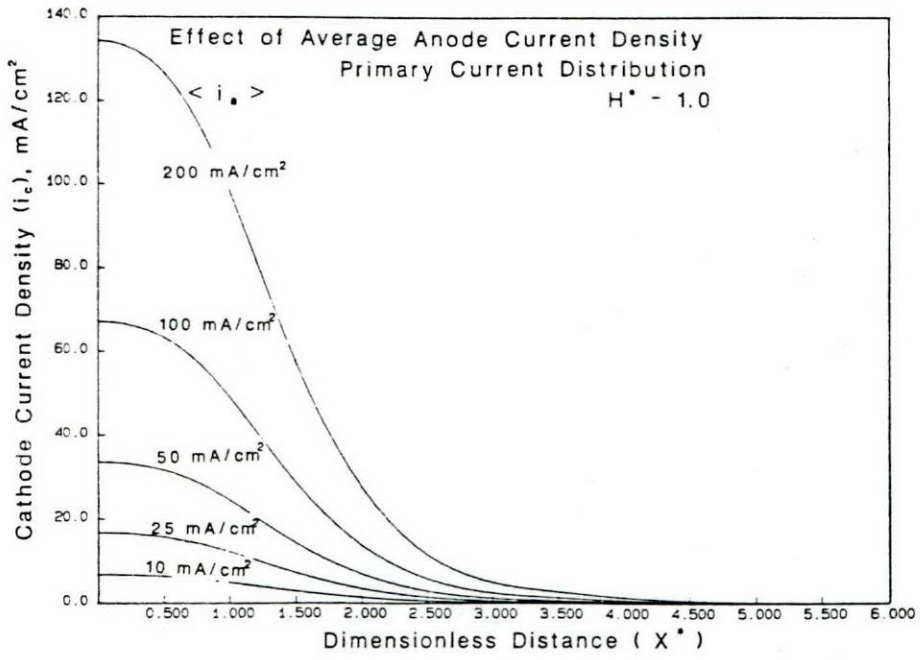

Figure 11. Calculated primary current distribution on a maskless cathode for gold plating from the acid hard gold bath.

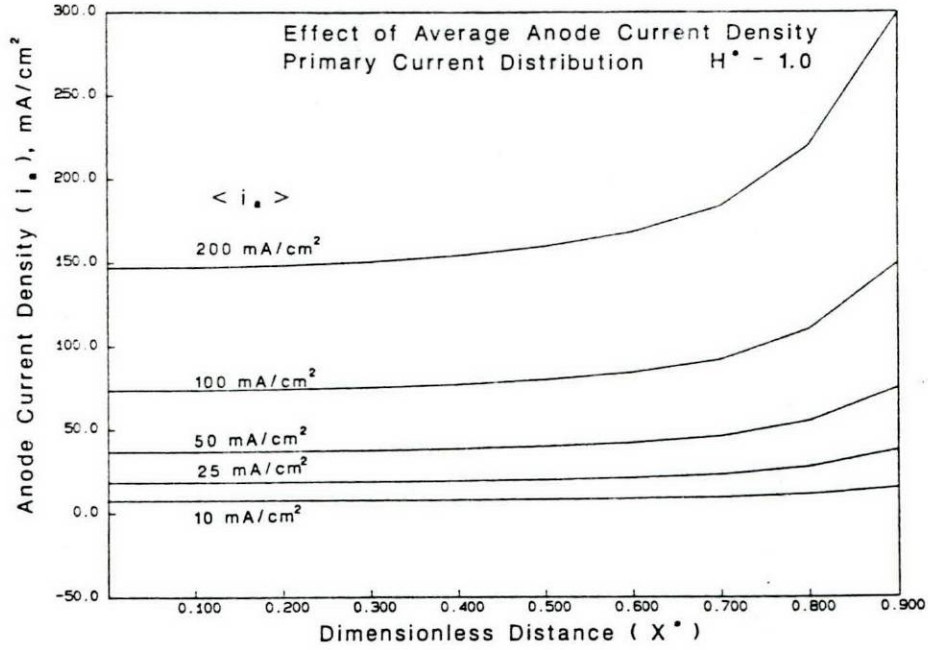

Figure 12. Calculated anodic primary current distribution for gold plating from the acid hard gold bath.

B-3

Research Session B

Thickness Effects on the Mechanical Properties of Electrodeposits

Ingon Kim and Rolf Weil
Stevens Institute of Technology
Hoboken, NJ 07030

THICKNESS EFFECTS ON THE MECHANICAL PROPERTIES OF ELECTRODEPOSITS

Ingon Kim and Rolf Weil

Stevens Institute of Technology, Hoboken, NJ 07030

INTRODUCTION

The mechanical properties of thin foils have been of interest to investigators since 1933 when Orowan (1) observed that thin mica sheets exhibited exceptionally high strengths. Since then most of the studies of the mechanical properties of thin foils have involved vapor deposits. Investigators of the properties of electrodeposits have generally only measured the hardness. No systematic study of the mechanical properties of electrodeposits which included those with thicknesses in the submicron range, where the greatest strength increase occurs in vapor deposits, has been performed. As part of the investigation of the mechanical properties of electrodeposits under AESF Research Project 69, the effects of deposit thickness were studied. Because of the initial design of a minitensile machine and a specimen for it carried out under AESF Project 38 (2), it was possible to test electrodeposits in simple tension which were as thin as 200 nm which is only about 1000 atom layers . The results of this study are reported here.

EXPERIMENTAL PROCEDURE

The substrates were pieces of cube-textured copper sheet i.e., most of the grains had a {100} crystal plane parallel to the surface. Photolithography was used to plate the tensile specimens directly to the desired shape. The surfaces of the substrates were coated with photoresist prior to plating. The mask having four cutouts in the shape of the tensile specimen shown in Figure 1 was then placed on the photoresist-coated substrate. The masks were placed on the substrate so that the prospective tensile direction was parallel to <012> in most grains. The mask also did not cover a 2 cm wide boarder. After exposure to ultra-violet light, the photoresist was developed so that it was dissolved in the areas exposed to the ultra-violet light. In this way, only areas having the shapes of the four tensile specimens were not insulated and thus could be nickel plated. The boarder was also not insulated so that when it was plated, the current density in the central region would be uniform. The uninsulated areas were electropolished in a 67% aqueous phosphoric-acid solution. After rinsing, they were plated in a solution containing 112 g/l $NiSO_4 \times 6H_2O$ and 30 g/l H_3BO_3 . The current density was 2.5 mA/cm^2 ; the pH was 4

and the temperature of the solution was 20C. The deposit thickness varied from 200 nm to 9.5 μm.

The specimen design shown in Figure 1 made it posssible to test deposits as thin as 200 nm. Specimens so thin would have been too weak to be handled after dissolving the substrates without additional support. Therefore while the deposits were still attached to the substrates, the gage-length portion was coated with an insulating laquer and the remaining area was futher nickel plated. This heavier plated area was painted black for illustrative purposes on the photograph which is Figure 1. The thicker deposit on the ends and on the segment parallel to the gage length acted as a supporting frame to prevent the thin portion from deforming.

After dissolving the copper substrate in a chromic-sulfuric acid solution, the specimens were mounted on the grips of the minitensile machine. The functioning of the minitensile machine was described previously (3). The segment parallel to the gage length of the tensile specimen was severed after mounting on the grips. After testing, the fractures were examined by transmission and scanning electron microscopy. Scanning electron microscopy and weighing were used to determine the specimen thicknesses.

RESULTS AND DISCUSSION

The mechanical properties of the nickel deposits are listed in Table 1. Each value is the average of at least three measurements. The values in parentheses are the variations in the individual measurements.

It is seen that Young's modulus is not significantly affected by the deposit thickness. The variations with deposit thickness are probably due to small thickness nonuniformities. The yield strength is seen to decrease with increasing thickness and that of the 200 nm-thick deposits is significantly larger than the other values. The high yield strength of the thinnest deposit is probably due to surface pinning of dislocations. Figure 2 shows no evidence of any dislocation motion even in the areas near the fracture. The decrease in the yield strength as the thickness increased was probably due to greater dislocation mobility and the activation of sources for their generation. The tensile strengths are seen to be relatively unaffected by the thickness of the deposits. The values remained constant probably because the increased activation of sources for dislocation generation in the thicker deposits resulted in greater rates of work hardening. The degree of dislocation immobility thus became essentially the same in all deposits.

Table 1

Mechanical Properties of Nickel Electrodeposits

Thickness (μm)	Young's Modulus (GPa)*	Yield Strength (MPa)#	Tensile Strength (MPa)	Percent Elongation
0.2	80 (3)	220 (5)	220 (5)	0
2.0	92 (1)	154 (3)	200 (5)	2.2 (0.2)
4.2	92 (0)	137 (7)	190 (6)	3.7 (0.2)
5.7	87 (1)	130 (11)	200 (7)	6.2 (0.2)
7.5	86 (3)	122 (8)	210 (13)	7.0 (0.1)
8.3	84 (2)	130 (8)	204 (4)	7.0 (0.3)
9.5	85 (2)	123 (7)	205 (5)	7.0 (0.2)

* 7 GPA = approx. 1 million psi. # 7 MPa = approx 1000 psi

The reason why the 200 nm-thick deposit had no ductility as manifested by the percent elongation can be seen in Figure 2. As already mentioned, there is no evidence of any dislocation motion, i.e., plastic deformation having taken place. The fracture occurred in the boundaries of the grains which had a {100} plane parallel to their surface. Fracture also occurred within a grain which had a {111} plane parallel to its surface. This grain was thinner than the others. The probable reason the <100>-oriented grain were thicker is that the fiber axis of nickel plated in an all-sulfate solution is <100>. A fiber texture developes because grains with its orientation grow faster than the others (4). Thus the <100>-oriented grains grew to a greater thickness than the ones with the <111> orientation. The smaller thickness led to a higher stress and fracture within the grain while the others failed in the grain boundaries which were also probably a little thinner.

After the maximum load from which the tensile strength was calculated, had been applied, the thickness was substantially reduced over a portion of the gage length. This phenomenon is called necking. The portion of the gage length over which necking occurred increased with increasing thickness. Most of the platic deformation occurred in the

necked portion. Therefore the increase in the gage length at fracture from which the elongation was calculated, depended on how long a portion underwent necking. The greater the portion of the gage length which plastically deformed and necked, the greater was the elongation.

All deposits, regardless of initial thickness, were about 200 nm thick just prior to fracture. This result is evident in Figure 3, which shows the fracture of the thickest deposit which was tested. Evidently, it was thin enough adjacent to the fracture to be transparent to the electron beam which means that there it was less than 200 nm thick. The fracture shown in Figure 3 occurred in a grain with a {100} plane parallel to it surface. It fractured along two mutually perpendicular <110> directions and therefore probably on {111} planes. The final thinning before fracture took place by mechanical twinning. The twins can be seen at the fracture edge in Figure 3.

If the reduction in area is taken as an indication of ductility, the thick deposits are extremely ductile. The apparent thickness prior to fracture of about 200 nm seen in Figure 3 yields a calculated reduction in area of 99%. Also the true stress at fracture, which is the load divided by the actual area, is very high. There was little change in the gage length between the application of the maximum load and when fracture occured. Therefore, it was not possible to determine the fracture load. If the load which caused fracture is assumed to be half the maximum one, the true fracture stress would be about 1000 MPa, i.e., five times the tensile strength. On the other hand, the true fracture stress of the very thin deposits which showed no necking, was the same as the tensile strength.

It can be concluded that very thin electrodeposits exhibit high yield strengths. While the tensile strength was essentially the same for all deposits, the true fracture stength increased with increasing thickness because of necking. The elongation increased with increasing thickness because a larger portion of the gage length deformed plastically. Because all deposits necked down to essentially the same thickness prio to fracture, the reduction in area increased with increasing thickness.

REFERENCES

1. E. Orowan, Z. Physik, 82 , 234 (1933).

2. M. Parente and R. Weil, Plating and Surf. Finish, 71 , 114 (5/1984).

3. I. Kim and R. Weil, Testing of Metallic and Inorganic Coatings, W. B. Harding and G. A. DiBari, Eds., ASTM STP 947, 11, American Society for Testing and Materials, Phila. PA.

4. R. Weil, Proc. Interfinish '84, 28 (1984)

ACKNOWLEDGEMENTS

The support of the Research Board of the American Electroplaters and Metal Finishers Society and its supporting members is gratefully acknowledged as is the advice of the members of the Project Committee consisting of Messrs. A. Damjanovic, G. Fisher, D. Hardesty, J. Horner, F. Koch, S. Nakahara, Y. Okinaka, T. Palumbo and M. Paunovic.

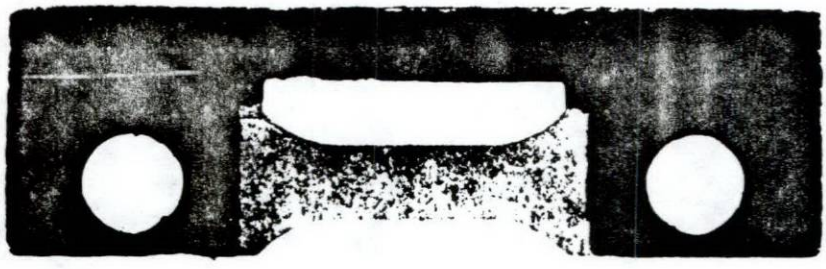

Figure 1. Tensile Spcimen. Blackened Areas were Plated Heavier When Deposits were thin.

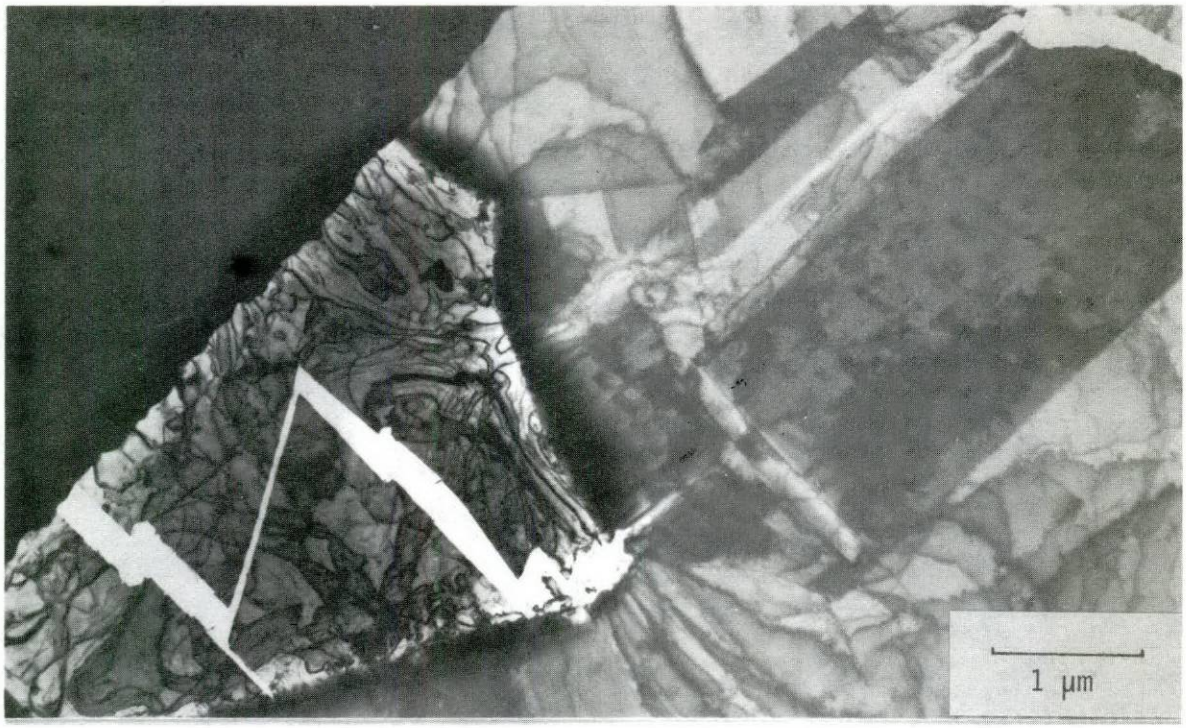

Figure 2. Fracture Region in 200 nm Thick Deposit.

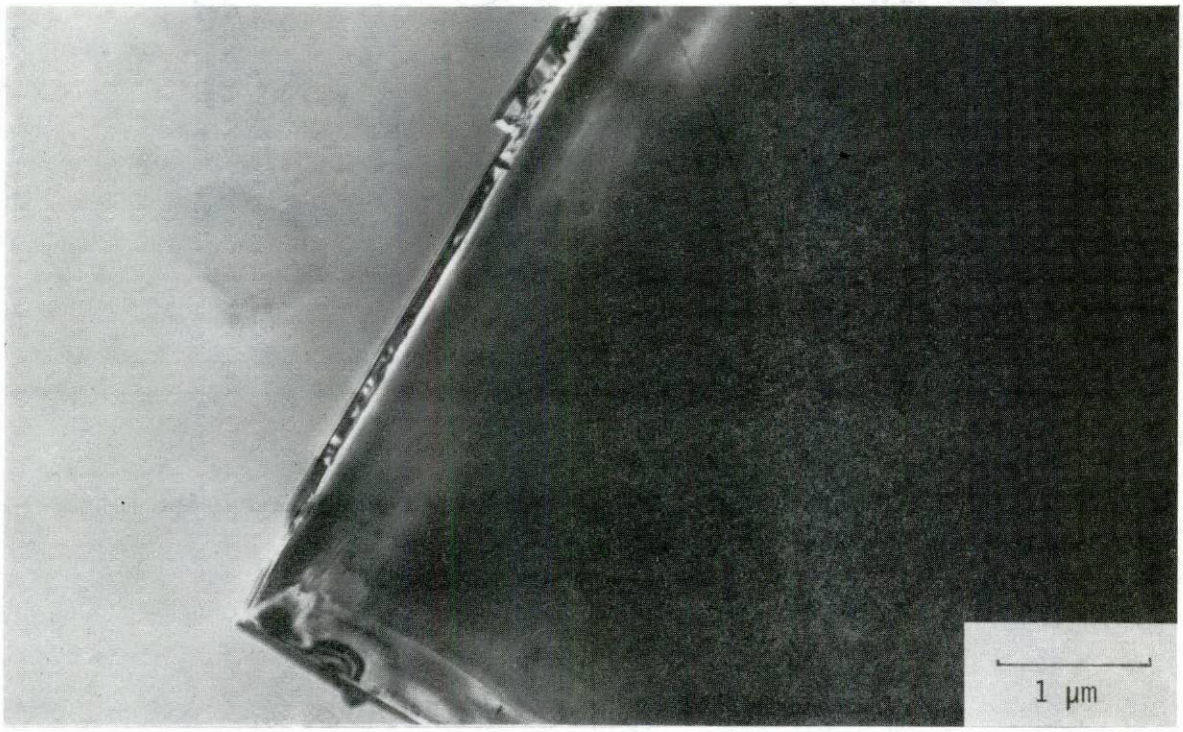

Figure 3. Fracture Region in 9.5 μm Thick Deposit.

B-4

Research Session B

Factors Affecting Low Temperature Interdiffusion

L. Giannuzzi, H.W. Pickering and W.R. Bitler
The Pennsylvania State University
University Park, PA 16802

Factors Effecting Low Temperature Interdiffusion

L. Giannuzzi, H. W Pickering, and W. R. Bitler
The Pennsylvania State University
University Park, PA 16802

Diffusion in crystalline solids can take place through the lattice and through the grain boundaries. It is believed that in most metals the mechanism of this diffusion is motion by interchange of atoms and vacancies. Because vacancies are present in higher concentration in the vicinity of grain boundaries and because these vacancies are more mobile than those in the lattice away from the grain boundaries, diffusion can take place at a faster rate in grain boundaries than in the lattice. There are two different aspects of grain boundary diffusion. First in a diffusion couple between two different chemical species, say for example between nickel and gold, the nickel can diffuse into the gold through the lattice and also through the grain boundaries and then into the lattice. If the time for diffusion is long enough for the diffusion from the grain boundaries into the lattice to completely penetrate the individual grains then the overall effect is the same as if there were only lattice diffusion but at a much higher rate than the diffusion rate would be in the absence of grain boundaries. Such an effect is indicated in Fig.1. This is a plot of the log of the diffusivity verses 1/T where T is the temperature in kelvins. The steep line to the left of the diagram which is continued as a dotted line is the diffusivity one would observe in a single crystal, i.e. in the absence of grain boundaries. The lines with lower slopes represent the contribution to the volume diffusivity arising from the presence of grain boundaries and as one would expect the effect increases with the number of grain boundaries, i.e. as the grain size decreases. Note that because this is a logarithm plot, this means that at low temperatures (the right side of the graph) the effective D determined for polycrystalline samples can be orders of magnitude larger than for a sample without grain boundaries. This project has examined a number of systems for this effect in the past and reported on them. To secure such data at low temperatures requires long diffusion anneals at low temperatures, sufficiently long such that the diffusion from the grain boundaries

into the grains effectively completely penetrates the grains.

It is apparent that the grain size plays an important role with the effect getting larger as the grain size decreases. In prior reports the effect of pH of the plating bath on the grain size of palladium deposits was reported for Pd electrodeposited from ammonia containing baths. As the pH was increased the grain size increased, but not uniformly. Instead a bimodal grain size distribution developed with increasing pH although the average grain size increased. The maximum pH realizable with this bath was a pH of 9. At higher pH the bath becomes unstable with the evolution of ammonia. Additional grain size data will be reported for Pd deposited from a bath not containing ammonia in which the pH can be extended up to a pH of 12.

A second effect is that at shorter diffusion times and/or at lower temperatures such that the diffusion into the grains from the grain boundaries may be negligible, there still may be significant diffusion along the grain boundaries over comparatively large distances. Thus at distances large compared to the grain size and large compared to the diffusion distance in the lattice from the original interface between two chemical species, again for example in a gold- nickel diffusion couple, the Ni penetration into the Au grain boundaries may be significant. Because the thickness of the grain boundaries is so small, of the order of Ångstroms, the amount of the diffusing species within the grain boundary is so small that it can not be detected by a microprobe. This does not mean however that the transport through the grain boundaries can be ignored. For example in a thin film, e.g. an electrodeposit, one may find that in terms of data obtained by a microprobe that the diffusion of the substrate into the electrodeposit has advanced only a small fraction of the way through the electrodeposit. However an examination of the free surface by techniques such as Auger spectroscopy may indicate that there has been penetration of the electrodeposit by grain boundary diffusion and a significant build up of the substrate material on the free surface. This surface build up of the substrate material can influence the surface properties such as the wettability of the surface and in turn effect such technologically important properties as solderability. It is the current goal of this project to

explore means to reduce the permeation of thin films by grain boundary diffusion. A promising avenue for such control is to introduce impurities in low concentrations that are segregated to the grain boundaries and effect the grain boundary diffusivity. Preliminary data on the effect of Bi on the grain boundary diffusivity of Au and Ni into copper will be presented.

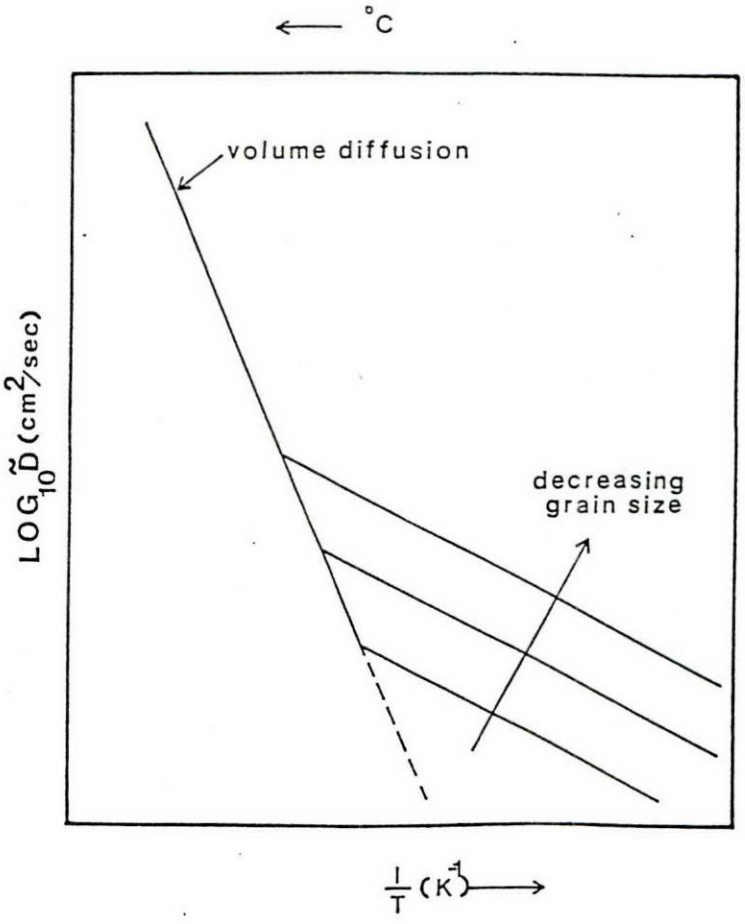

B-5

Research Session B

Effects of Additives in Acid Chloride Zinc Deposition

T.J. O'Keefe, J.S. Cuzmar
and Y.S. Park
Graduate Center for Materials Research
University of Missouri-Rolla
Rolla, MO 65401

S. Wagner
Missouri Electrochem Inc.
10958 Lin-Valle Drive
St. Louis, MO 63123

EFFECTS OF ADDITIVES IN ACID CHLORIDE ZINC DEPOSITION

T. J. O'Keefe, J. S. Cuzmar, Y. S. Park
Graduate Center For Materials Research,
University of Missouri-Rolla, Rolla, MO 65401

S. Wagner
Missouri Electrochem Inc.,
10958 Lin-Valle Drive, St. Louis, MO 63123

Abstract

The effect of additives on morphology, crystal orientation, and polarization behavior for zinc deposition onto steel substrates from chloride solutions was investigated. Cyclic voltammetric techniques showed the polarization to be strongly dependent on both the wetting and brightening agents. The influence of agitation on the deposit was also studied.

1. Introduction

Electrodeposited zinc coatings are used extensively to provide improved corrosion resistance for steel. In addition to providing cathodic protection to the underlying metal, the plated pieces are attractive in appearance as a result of the variety of bright zinc systems developed by the metal finishing industry. Any number of zinc plating technologies are available and include cyanide, alkaline, and acid chloride based electrolytes [1,2]. Each process offers different advantages in performance, ease of operation, effluent treatment, and overall economics and efficiency. The final selection must then be made by choosing a process which most closely meets the criteria as they relate to the final end use [3]. Some excellent descriptions of the zinc plating processes have been given and further elaboration will not be made in this paper. However, an area that seems to have received little attention is the polarization characterization of the zinc deposition process.

One major objective of this work, which was sponsored in part by the AES, was to initiate studies on determining various electrochemical aspects of the process. In particular, the behavior of two prominent additives in the zinc chloride process [4], a surfactant and a brightener were evaluated. Cyclic voltammetry techniques were used to generate polarization curves on the system. Galvanostatic deposits at a fixed current density and Hull cell tests were also made. In addition to providing fundamental information about the process, the research was directed toward determining the possibility of using electrochemical tests for electrolyte and additive analysis and plating bath characterization [5,6]. Deposits were made using synthetic electrolytes and beaker cells at the University of Missouri-Rolla (UMR) laboratories, while commercial electrolytes were used for zinc deposition for the industrial tests. Duplicate deposition tests and exchange of materials was employed to insure that any results obtained might more likely be correlated with industrial practice.

2. Experimental

2.1. Electrodeposition System

Synthetic solution was prepared by dissolving 44.94 g/l zinc chloride, 112.34 g/l potassium chloride, and 25 g/l boric acid in deionized water. All solutions were filtered to remove suspended impurities prior to use. The pH was about 5.2, and the temperature was maintained at 27°C during the tests by immersing the cell in a water bath.

AISI 1008 low carbon steel strips, 19 mm x 76 mm, were used as the starting cathode substrate. The strip was first cleaned ultrasonically in laboratory grade detergent, rinsed with deionized water, dried with absorbent paper, and degreased in trichloroethylene. The electrodes were covered with plater's tape to give a circular 1 cm^2 area to be plated. The exposed area was then anodically cleaned at 100 mA/cm^2 at 60°C in 15 g/l proprietary alkaline cleaner for 30 seconds, dipped into the 1 M hydrochloric acid for 30 seconds, rinsed with deionized water, and dried in a stream of nitrogen.

For the cyclic voltammetry experiments, AISI 1008 low carbon steel rod with 1 cm^2 cross sectional area was mounted in an epoxy resin, polished with 600 grit silicon carbide paper, rinsed, and dried in a stream of nitrogen before immersing into the electrolyte. The pure zinc anodes, 26 mm x 110 mm, were cleaned ultrasonically in 0.5 M hydrochloric acid for 30 seconds, rinsed, and dried prior to use. The cell for the plating and cyclic voltammetry tests consisted of a 250 ml beaker, with a plexiglass lid with provisions for mounting the cathode, the anode, and the reference electrode. The anode to cathode spacing was 25 mm for deposition tests and 30 mm for the cyclic voltammetry tests; 200 ml of electrolyte was used. The steel substrate was held in the electrolyte for 15 seconds prior to plating to provide time for an equilibrium condition to be established. Most of the galvanostatic deposits were made at a current density of 35 mA/cm^2. After 10 minutes deposition, the cathode was removed from the cell, rinsed, and dried with nitrogen for further study by SEM and x-ray diffraction for morphology and orientation.

2.2. Hull Cell Test

For the Hull cell deposition tests, both carbon filtered and unfiltered electrolyte were used, but initial results showed no difference between them. A standard low carbon steel panel (10 x 6.6 cm) was used for the cathode.

The amount of electrolyte was 267 ml, which contained 45 g/l zinc chloride, 123.57 g/l potassium chloride, and 24.34 g/l boric acid. The pH was about 5.2 and the plating tests were made at room temperature for 5 minutes using a current of one ampere. The electrolyte was agitated in some tests, as well.

To examine the zinc deposits from the Hull cell tests, the steel panels were cut into sections representing the various current densities. Samples

at a current density of 35 mA/cm^2 were used most often for SEM and x-ray diffractometer examination.

2.3. Potentiodynamic Test

The polarization curves were generated using a low carbon steel working electrode which was allowed to stay at open circuit potential for 15 seconds prior to initiating the scan. The cyclic voltammetry scans started at -0.85 V vs. SCE at a rate of 5 mV/sec, and the direction was reversed at -1.35 V vs. SCE.

2.4. Additives

Various additives were used in the study. Included were an anhydrous, liquid non-ionic surface agent produced by the reaction of nonylphenol with 10.5 moles of ethylene oxide (Surfactant I), a 70% active solution made from a non-ionic surface active agent produced by the reaction of nonylphenol with 30 moles of ethylene oxide (Surfactant II), and a commercial non-ionic Surfactant III were used as the wetting agents. Ortho-chlorobenzaldehyde, and commercial brightener were used in combination with the surfactants.

3. Results and Discussion

3.1. Deposit Morphology

The synthetic solution without additives gave a light grey, level deposit at 35 mA/cm^2 current density, 27°C for 10 minutes plating time. The morphology of the deposit is shown in Figure 1. A sample was taken at the 35 mA/cm^2 position from a deposit made in a Hull cell using industrial solution, and the morphology is shown in Figure 2. Additional tests are planned to see if there are any subtle changes that might emerge due to the difference in purity of the various chemicals used or if the finer grain size on the Hull cell deposit is more a function of the deposition method employed.

Upon the addition of various non-ionic wetting agents, a finer grained structure was obtained, compared to the structure from addition-free electrolyte. Generally, as the amount of wetting agents increased, the deposit become a darker grey to brown color, and a nodular finely dendritic structure was obtained. Figures 3, 4, and 5 show the structures obtained for the three surfactants used. The deposits for Surfactant I and III were similar, both showing a uniform dense deposit, but probably with a microscopic surface roughness. Both appeared to be a brownish color in reflected light. Surfactant II gave a needle-like, dendritic growth with a very open and non-continuous growth and was dark grey in color.

The concentrations for the wetting agents were in the range of 0.3% in volume for Surfactant I and II, and 1.5% in volume for Surfactant III. Commercial brightener and ortho-chlorobenzaldehyde were added in the concentration range of 0 to 0.3% for commercial brightener and 0 to 50 ppm for ortho-chlorobenzaldehyde to electrolyte containing the surfactants. These concentrations were suggested by the suppliers and users of the chemicals.

As the amount of brightener increased, more hydrogen evolved at the cathode surface, particularly with Surfactant I, but smooth bright deposits were obtained, once sufficient brightener was present. In some cases, a striated appearance occurred, probably due to the hydrogen gas streaming across the cathode surface. Figure 6 shows that 1.5% Surfactant III with 0.15% commercial brightener gave a smooth, dense deposit, and with agitation a similar and even brighter, smoother deposit was obtained (Figure 7). When the brightener content was increased to 0.3%, a nodular deposit was produced and extensive gas evolution was evident during plating (Figure 8). When the electrolyte was agitated, the deposit remained bright, even at the higher brightener concentration, but some sub-micron pitting was noticed, as shown in Figure 9. Figure 10 shows that 0.3% Surfactant I with 15 ppm ortho-chlorobenzaldehyde also gave a reasonably good deposit but a slight discoloration was noticed with time.

It is well known that the wetting agent and brightener concentrations are important to obtaining quality deposits [7,8]. The morphology results reveal not only the need to maintain a proper balance of surfactant to brightener, but that this ratio is then influenced by the relative degree of agitation, and must be considered when establishing the operating parameters used for the process.

3.2. Deposit Orientation

Table 1 shows the crystal orientations of the zinc deposited from the solutions of addition-free, surfactant, and surfactant plus brightener. Without additives, the deposit made from synthetic electrolyte was strongly (110) and (101) oriented. The Hull cell deposit gave a dominant (101) orientation. The orientation of deposits made with only surfactants present gave stronger (100) peaks in addition to the (101), and a noticeable increase in the (002) as well. When the deposits made with surfactant and brightener were smooth and bright, the intensity of the (002) was noticeably low (0-12%), but in the case of the dark grey deposit, the (002) intensity was higher than about 17%. Agitation did not change the preferred orientation of the deposits.

3.3. Polarization Behavior

Representative polarization curves for addition-free, synthetic and industrial electrolytes, with and without agitation, are given in Figure 11. Very roughly, the curves are similar up to about 10 mA/cm^2, indicating there is little mass transport dependency at a current density lower than this value. Without agitation, a limiting current density of 45 mA/cm^2 is noted. A limiting current density of 100 mA/cm^2 was obtained with 500 rpm stirring speed. The curves indicate that additional fundamental information on the mass transport characteristics on this system might prove valuable in gaining better insight into the acid zinc chloride system. The anodic portion of the curves shows little or no diffusional control involved during zinc dissolution.

The presence of the three surfactants in the synthetic electrolytes caused an increase in the polarization, as indicated in Figure 12. A

characteristic current plateau was obtained for each in the forward scan, probably due to the strong influence of the initial absorption of the organic on the working electrode. The apparent limiting current density was also significantly decreased, but less for Surfactant III than the other two. The front sweep portion of the curve is indicative of the nucleation overpotential needed to initiate zinc deposition on the steel substrate. The curve is less polarized on the reverse sweep and is more of an equilibrium condition, since zinc is now depositing on a zinc surface. The degree of hysteresis observed is an indication of the relative differences between the overpotentials for zinc nucleation and growth. The relative overpotentials at 10 mA/cm^2 resulting from increasing amounts of each of the surfactants are given in Figure 13. The polarization is highest for Surfactant III, with increases noted up to concentrations of 1.5%. Those for the other two are much less and reach a constant value of 0.3%. The exact significance of these values is not known, but it is interesting to observe that the concentrations suggested for use, correspond to the approximate values at which no further increase in polarization is observed. From the curves in Figure 14, the polarizing effect of Surfactant III is seen to be a function of the concentration added.

When a combination of 0.3% Surfactant III and varying amounts of commercial brightener were added to the solution, considerable nucleation overpotential occurred (Figure 15). The magnitude of the initial polarization was related to the brightener content, with larger values occurring as the concentration increased from 0.03% to 0.2%. Some increase in polarization was observed on the reverse scan, and again was dependent on the brightener concentration, but to a lesser degree. The anodic curve also showed a polarizing effect which appeared to be a function of the brightener concentration.

When the surfactant is increased from 0.3% to 1.5% on even greater increase in nucleation overpotential occurs and is proportional to the amount of brightener present (Figure 16), change also is noted in the reverse sweep portion, with considerably more and approximately linear polarization behavior observed. The amount of overpotential is also related to the brightener concentration in this portion of the curve.

Polarization behavior with and without agitation for solutions containing 1.5% Surfactant III plus various amounts of commercial brightener is shown in Figure 17. All the curves are for the reverse scan direction. An interesting combined effect of the polarizing effect of the additives with the depolarization due to the enhanced mass transport caused by agitation is observed. The data indicate that the relative amount of active additive present at the deposition surface is strongly dependent on degree of agitation. The change in overpotential with stirring, at the various concentrations of brightener, is also much greater than when the electrolyte is quiescent.

When ortho-chlorobenzaldehyde was used with the commercial surfactant, a polarization behavior similar to that for the commercial brightener was obtained in the back sweep direction. The magnitude of the polarization was also increased as the amount added increased. However, the curve was

substantially different from the one generated when only surfactant was present.

4. Summary and Conclusion

Hull cell and beaker cell deposition tests have been conducted in an attempt to more clearly identify parameters of electrochemical importance in acid zinc chloride plating. The various surfactants used were found to be fairly strong polarizers, and then concentrations, in turn, determined the effectiveness of the brightener. The system was strongly mass transport dependent with an interesting relationship being observed between concentration and activation polarization with increasing current density.

In general, both additives exhibited strong polarizing effects, the degree observed being a function of the concentration. Although considerably more research is needed to more clearly elucidate the role of the various parameters, preliminary results on the use of polarization techniques for analyzing and characterizing the zinc chloride system are encouraging.

5. References

[1] H. G. Creutz and S. Martin, "Zinc Plating-Present Technology and Future Trends", Plating And Surface Finishing (1975).

[2] H. Geduld, "Zinc Plating", Metal Finishing (1986).

[3] V. K. Kansupada, "Zinc Plating Technology-Which Option Is Best For You ?", Finisher's Management (1985).

[4] M. P. D'angelo, "Chloride Zinc Plating", Products Finishing Directory (1987).

[5] B. A. Lamping and T. J. O'Keefe, "Evaluation of Zinc Sulfate Electrolytes by Cyclic Voltammetry and Electro Microscopy", Metallurgical Transactions B (1976).

[6] T. J. O'Keefe, "Techniques for Evaluating Electrolytes for Metal Recovery", J. Electroanal. Chem., 168 (1984).

[7] S. Martin, A. Z. Cutler and R. H. Bauer, "Recent Applications Of Acid Zinc Technology On A Commercial Scale", AES Paper (1985).

[8] R. Sard, "Advances in Functional Zinc And Zinc Alloy Coatings", Plating and Surface Finishing (1987).

Table 1. The Preferred Orientation and Appearance of the Deposits from the Synthetic Electrolyte without Agitation.

	(002)	(100)	(101)	(110)	(201)	(Appearance)
Random	53	40	100	21	17	
Addition-free	17	21	91	100	19	light grey
Surfactant I[2]	21	48	100	28		brown
Surfactant II[2]	42	37	100	41		brown
Surfactant III[2]	19	100	96		24	brown
Surfactant I[2] & co. brightener[1]	22	47	100	48		striated, gas evolution
Surfactant II[2] & co. brightener[1]		64	100	27	14	bright
Surfactant III[2] & co. brightener[1]		55	100	14	16	bright
Surfactant III[3] & co. brightener[1]	12	71	100	95	29	bright
Surfactant I[2] & o-CB[4]	17	59	100	43		brown
Surfactant I[2] & o-CB[5]	7	56	100	49	17	bright
Surfactant II[2] & o-CB[4]	45	41	100	49		dark grey
Surfactant II[2] & o-CB[5]	4	62	84	100	21	bright

1 : 0.15% 2 : 0.3% 3 : 1.5% 4 : 1 ppm 5 : 15 ppm

Surfactant I : nonylphenol with 10.5 moles of ethylene oxide
Surfactant II : 70% active solution of non-ionic surface active agent of nonylphenol with 30 moles of ethylene oxide
Surfactant III : commercial non-ionic surface active agent
Co. brightener : commercial brightener
o-CB : ortho-chlorobenzaldehyde

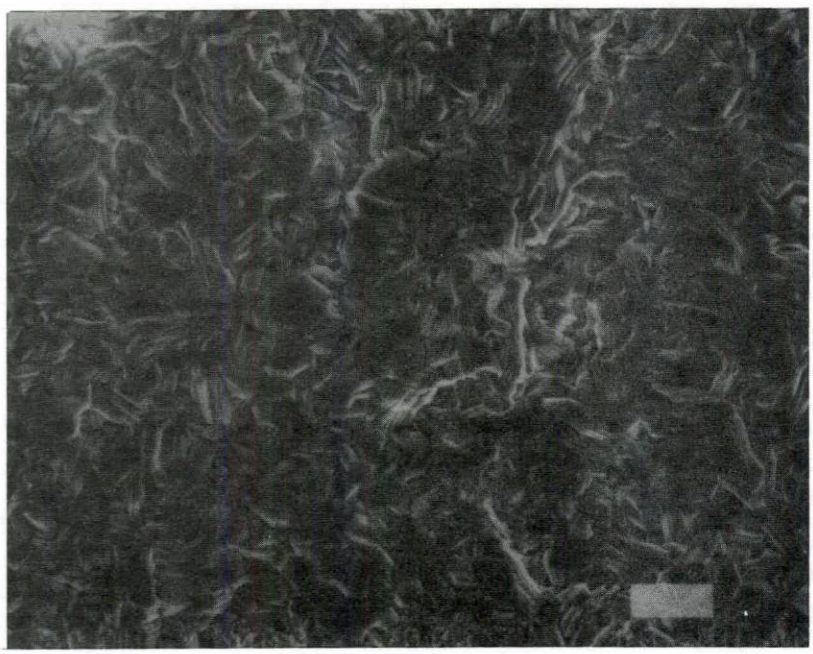

Figure 1. Zinc deposit from addition-free synthetic electrolyte, 1000x.

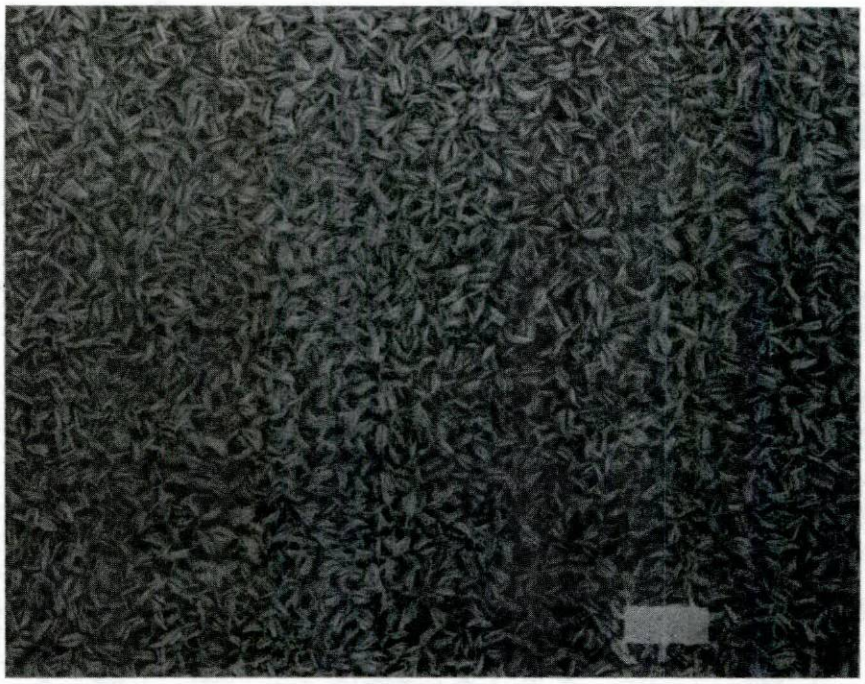

Figure 2. Zinc deposit from addition-free industrial electrolyte, 1000x.

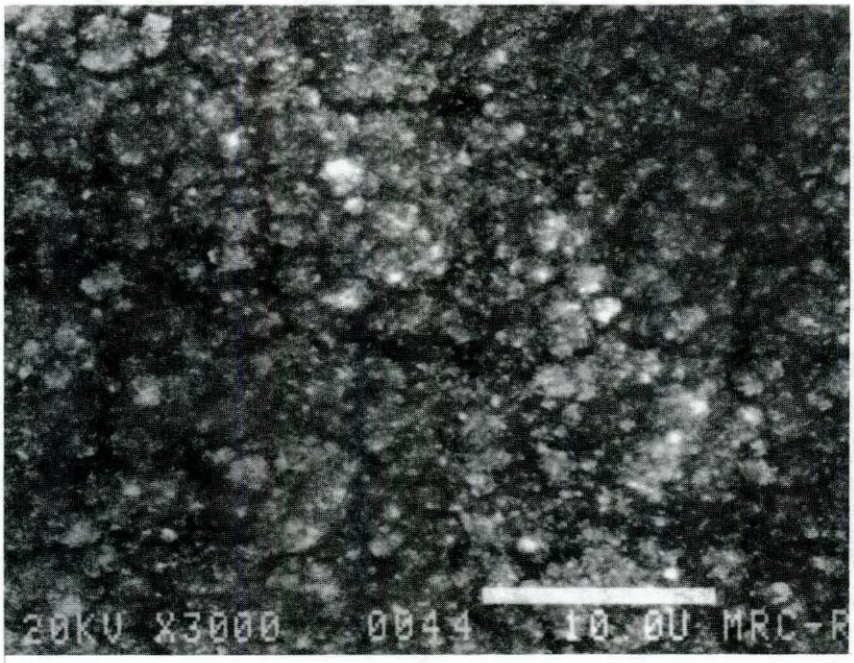

Figure 3. Zinc deposit from synthetic electrolyte containing 0.3% Surfactant I, 3000x.

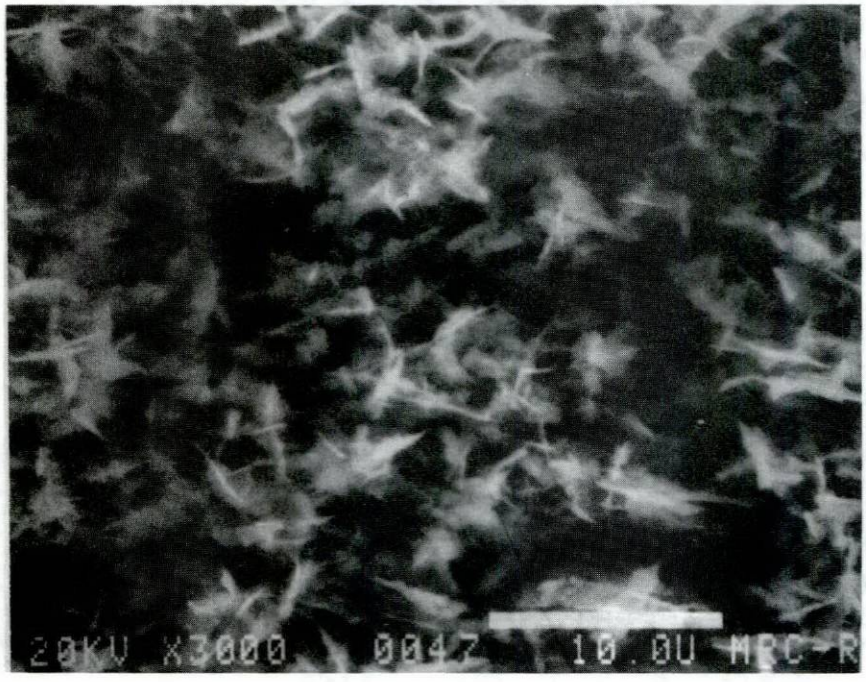

Figure 4. Zinc deposit from synthetic electrolyte containing 0.3% Surfactant II, 3000x.

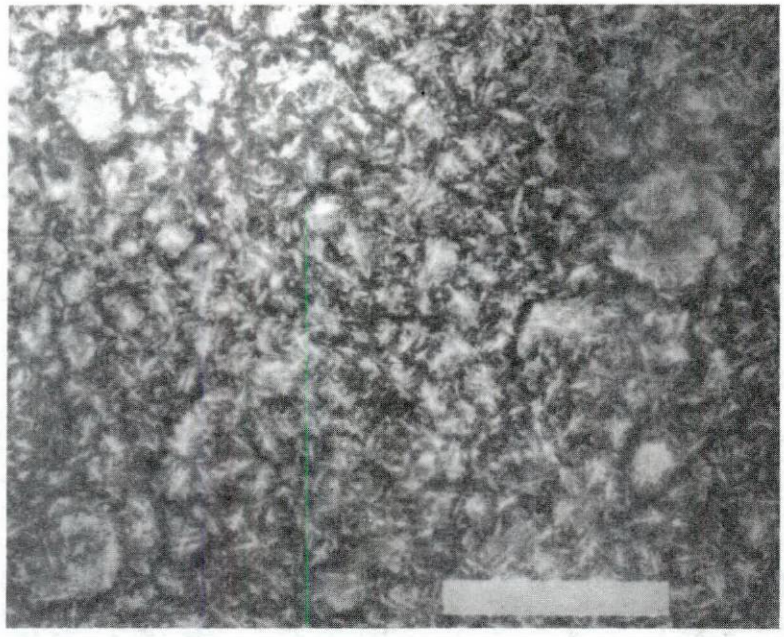

Figure 5. Zinc deposit from synthetic electrolyte containing 0.3% Surfactant III, 2000x.

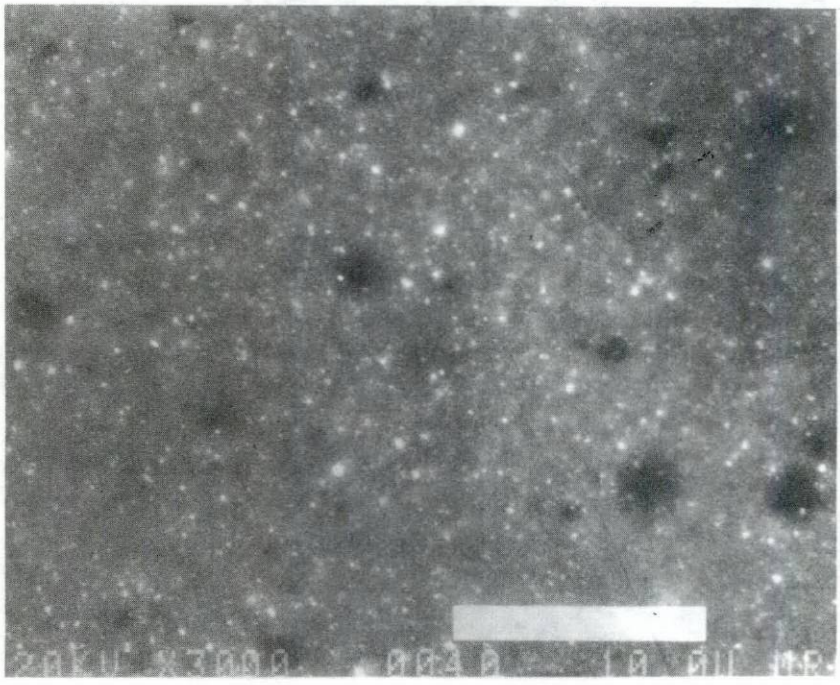

Figure 6. Zinc deposit from synthetic electrolyte containing 1.5% Surfactant III and 0.15% commercial brightener, 3000x.

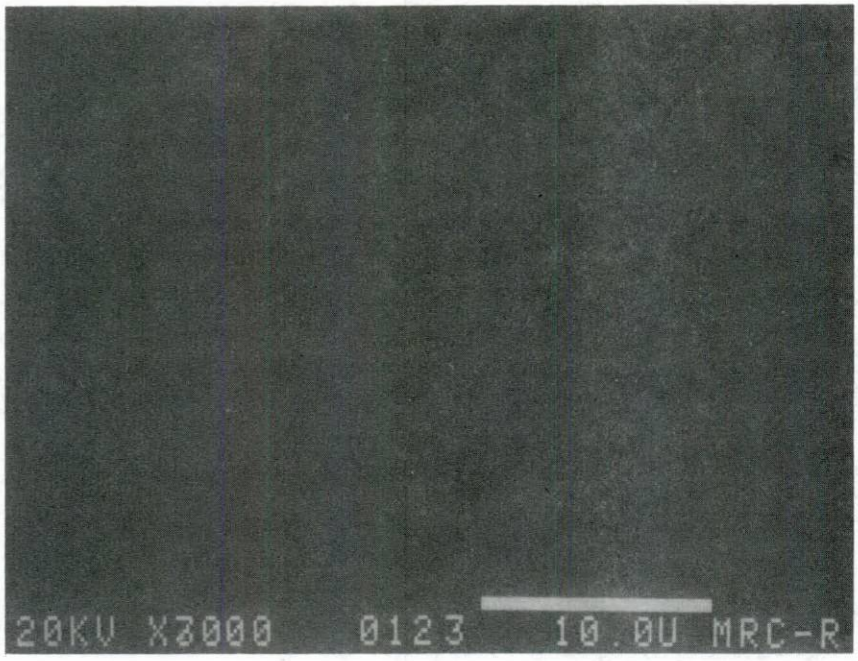

Figure 7. Zinc deposit from synthetic electrolyte containing 1.5% Surfactant III and 0.15% commercial brightener at 500 rpm stirring, 3000x.

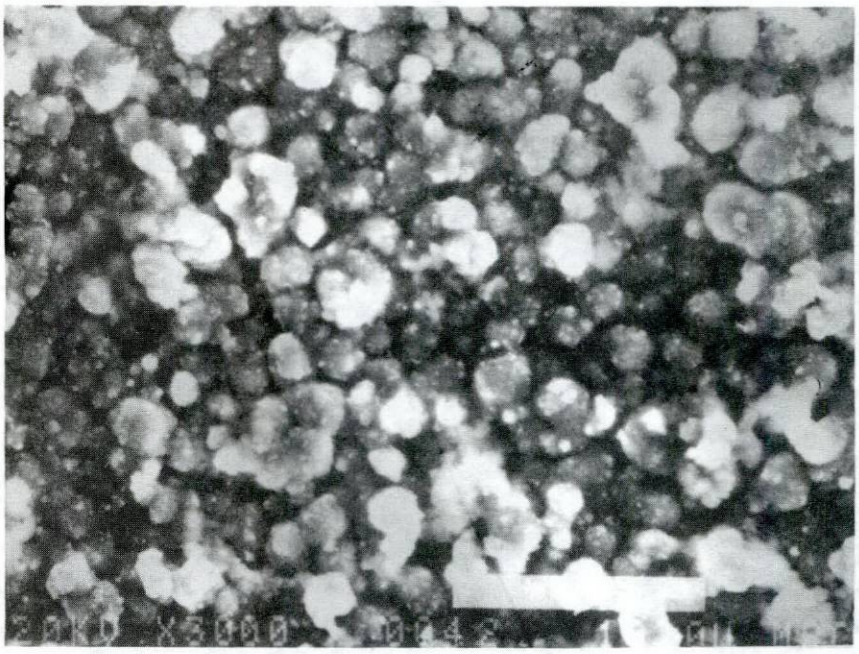

Figure 8. Zinc deposit from synthetic electrolyte containing 0.3% Surfactant III and 0.3% commercial brightener, 3000x.

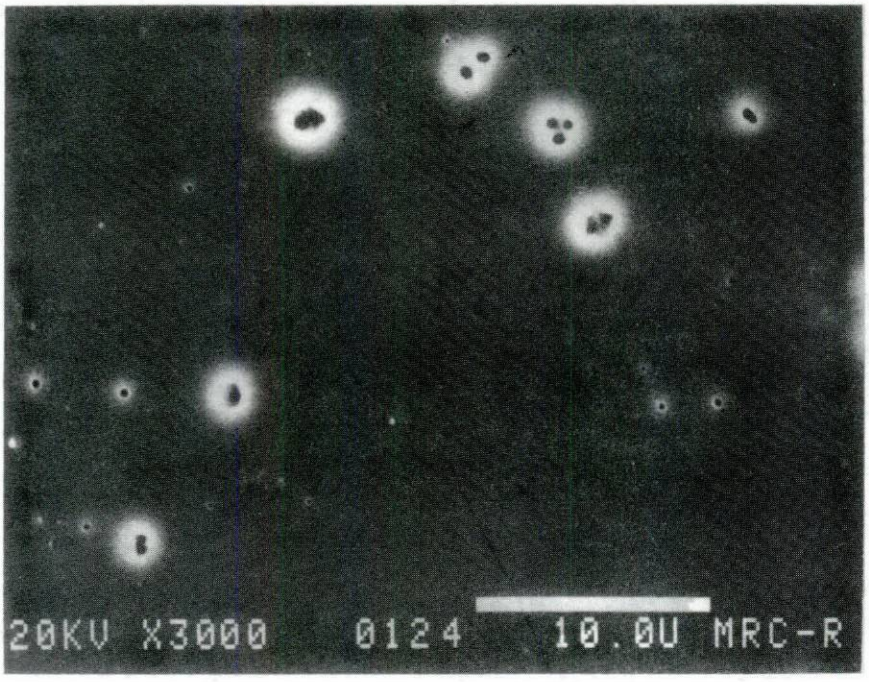

Figure 9. Zinc deposit from synthetic electrolyte containing 1.5% Surfactant III and 0.15% commercial electrolyte at 500 rpm stirring, 3000x.

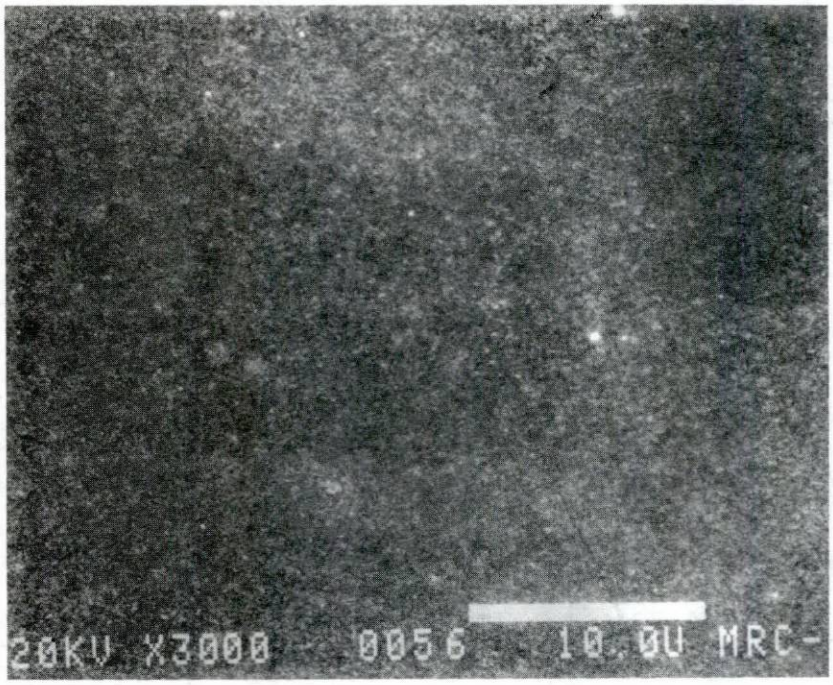

Figure 10. Zinc deposit from synthetic electrolyte containing 0.3% Surfactant I and 15 ppm ortho-chlorobenzaldehyde, 3000x.

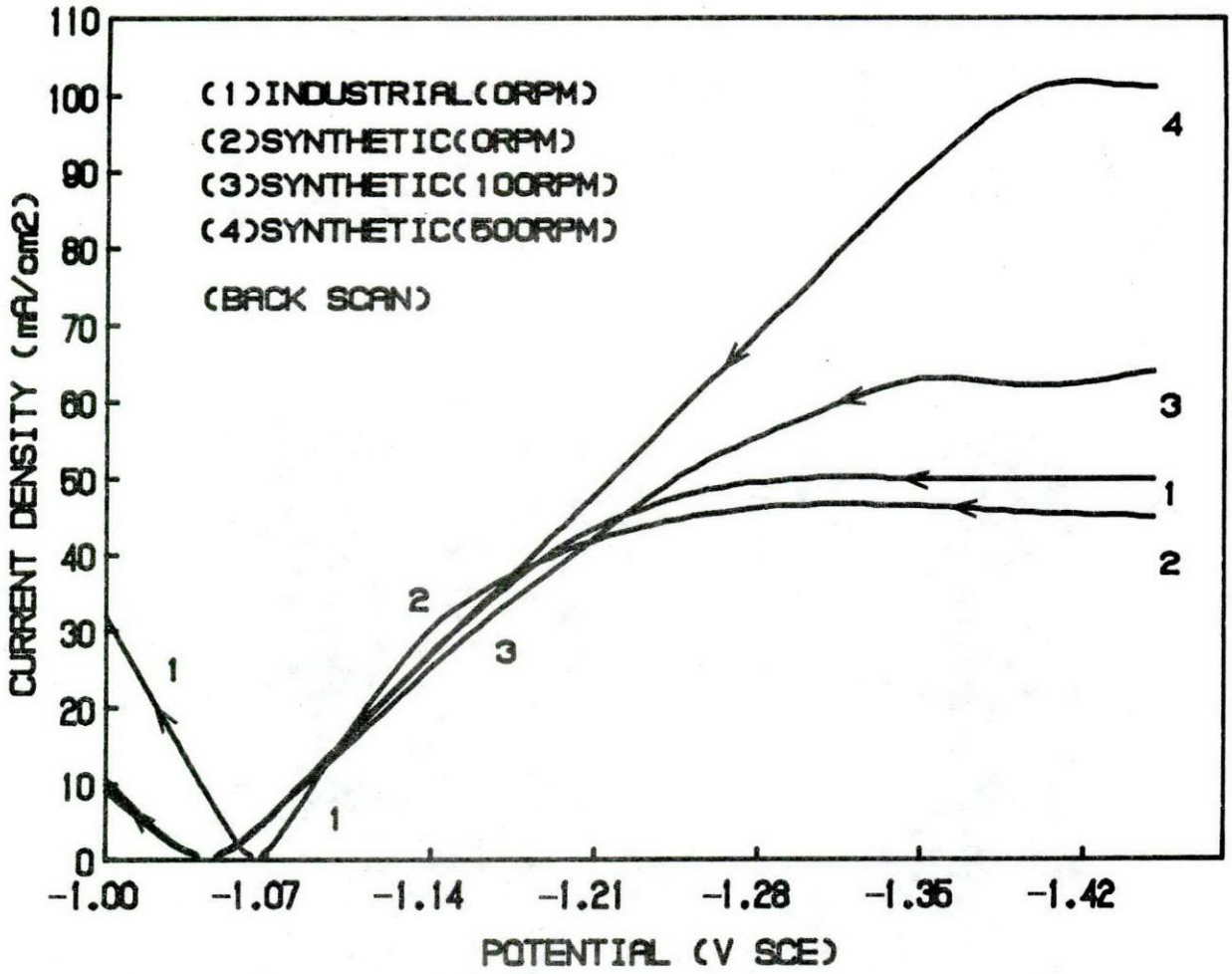

Figure 11. Polarization curves (back scan) of addition-free industrial and synthetic electrolytes with and without agitation.

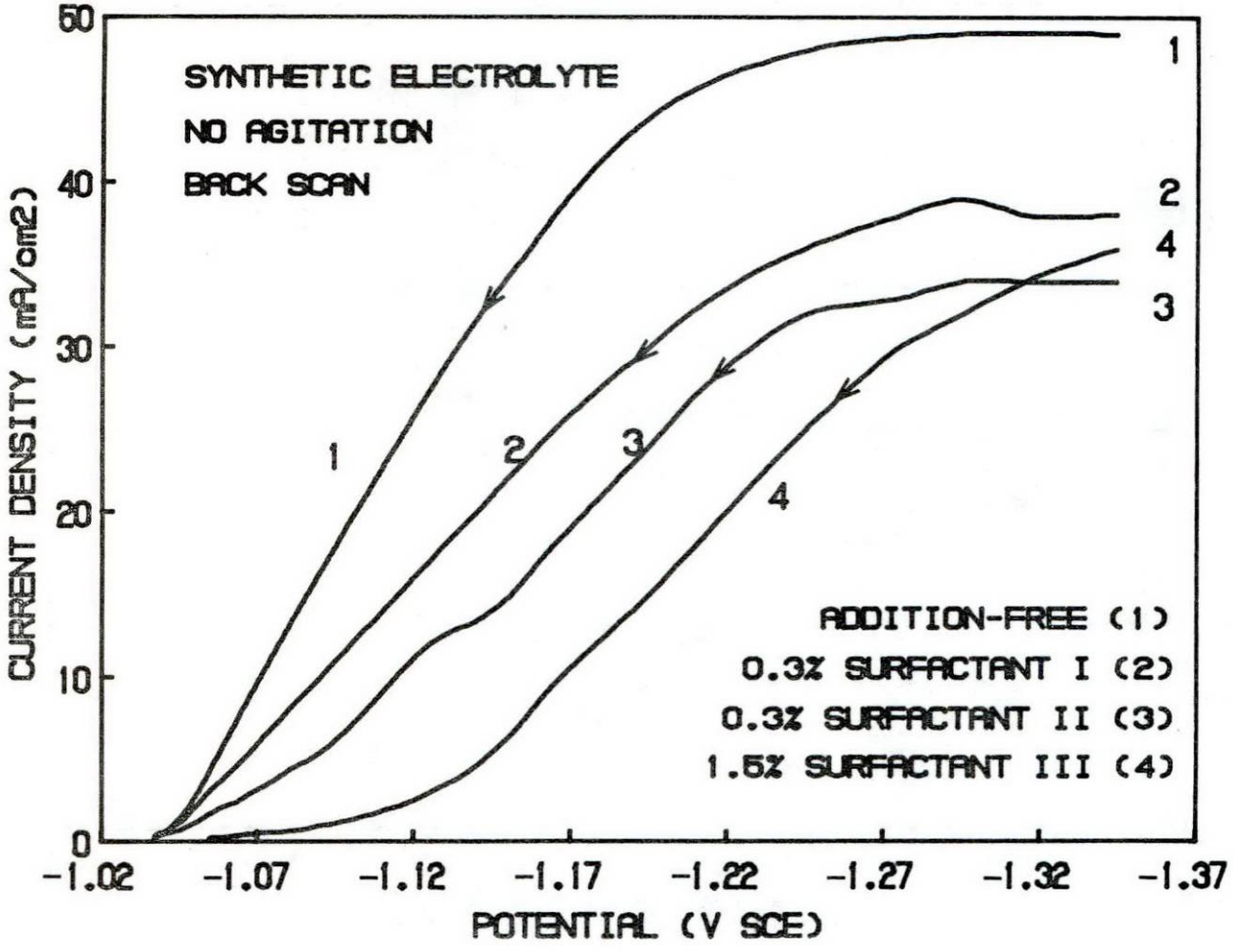

Figure 12. Polarization curves (back scan) for synthetic electrolyte containing different surfactants.

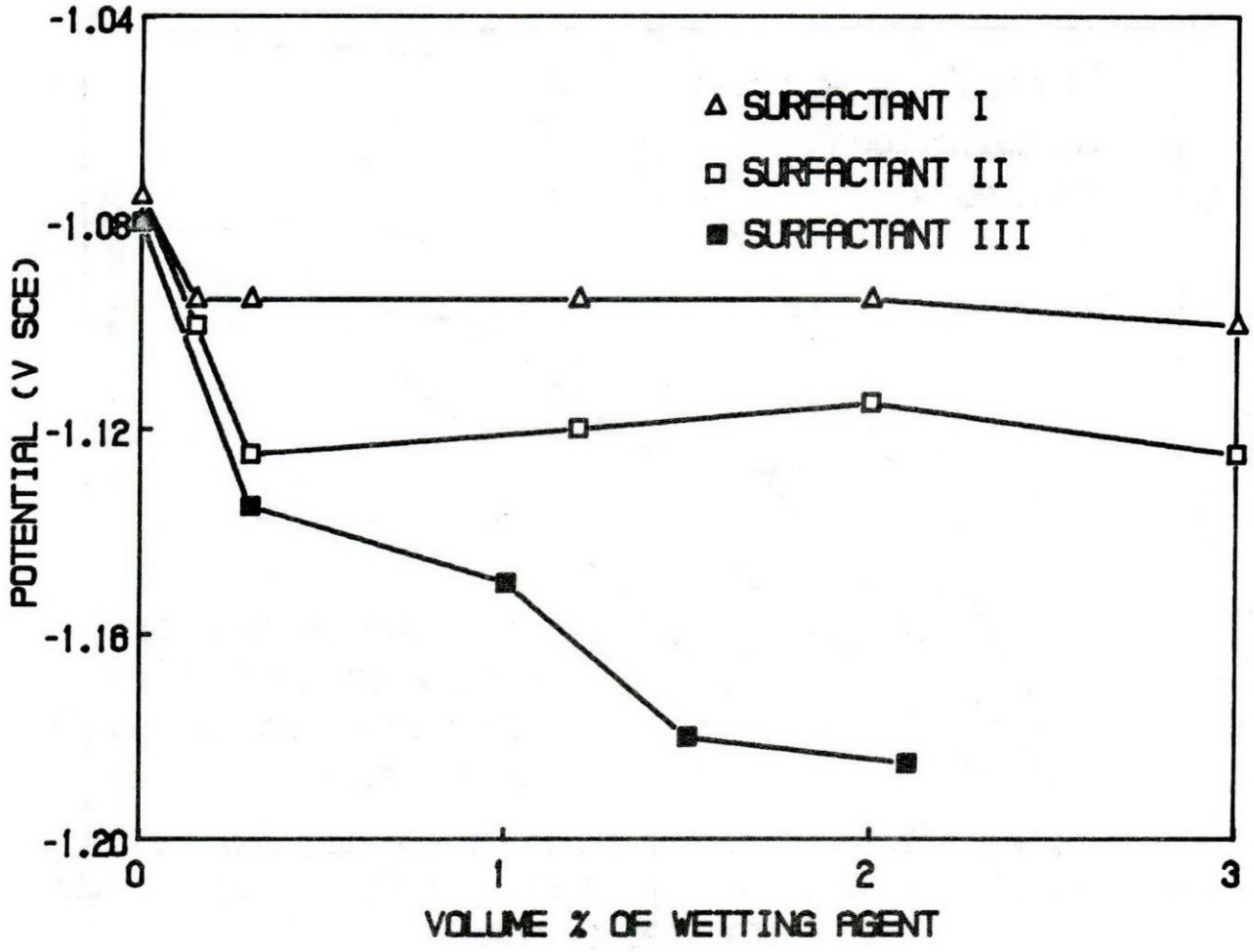

Figure 13. Overpotentials at 10 mA/cm^2 resulting from various concentrations of surfactants in synthetic electrolyte.

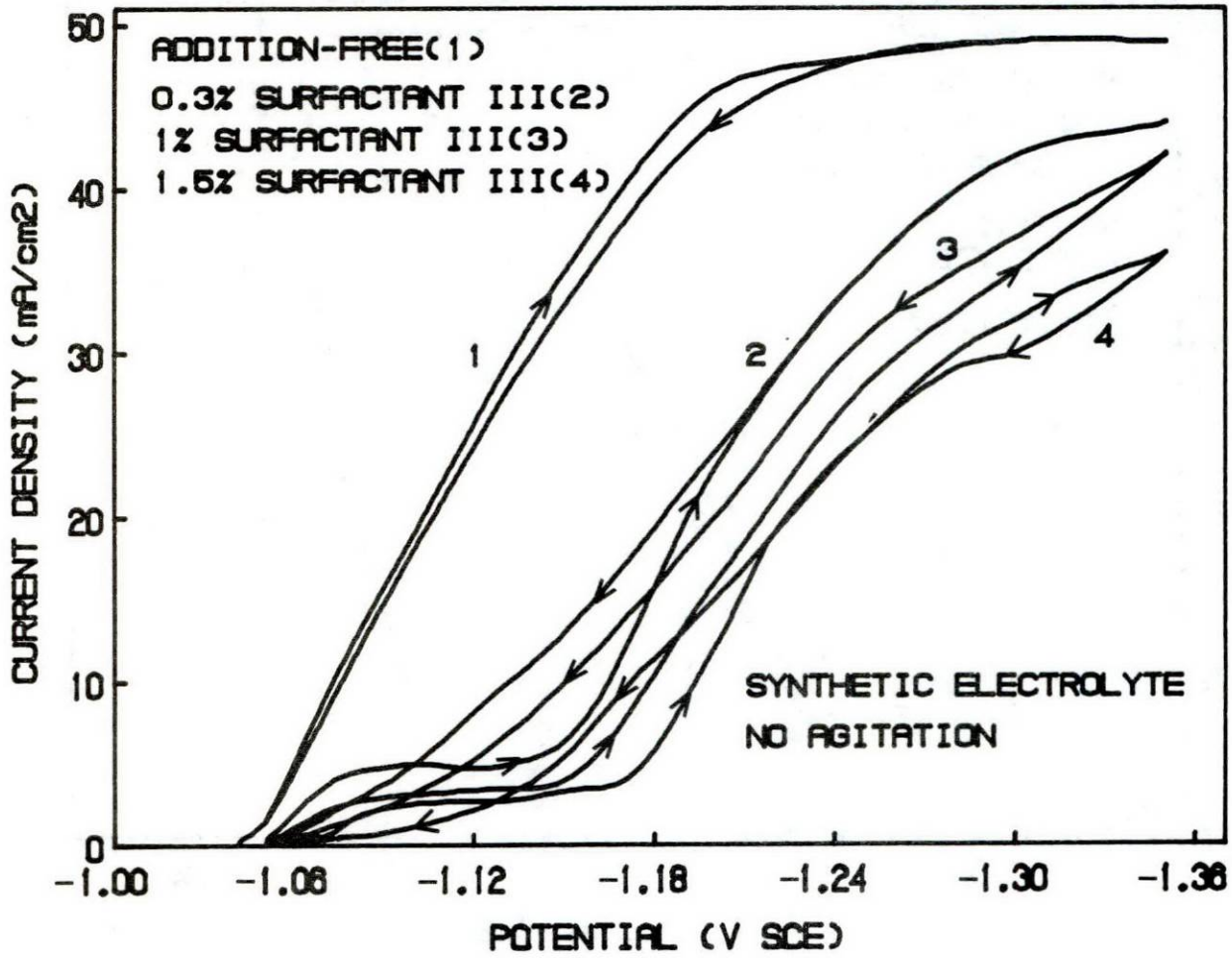

Figure 14. Polarization effects of different concentrations of Surfactant III in synthetic electrolyte.

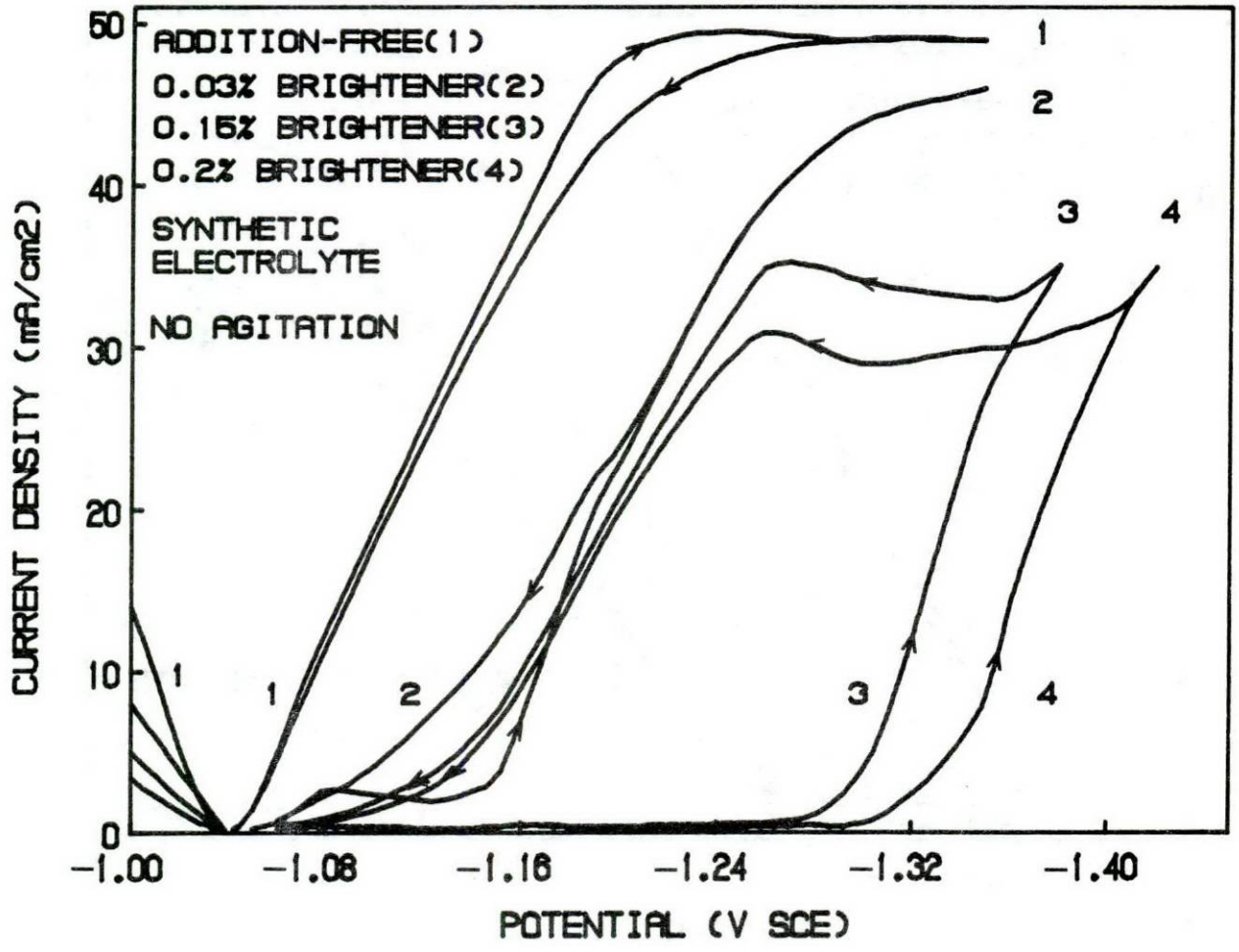

Figure 15. Polarization effects of 0.3% Surfactant III with varying concentrations of commercial brightener in synthetic electrolyte.

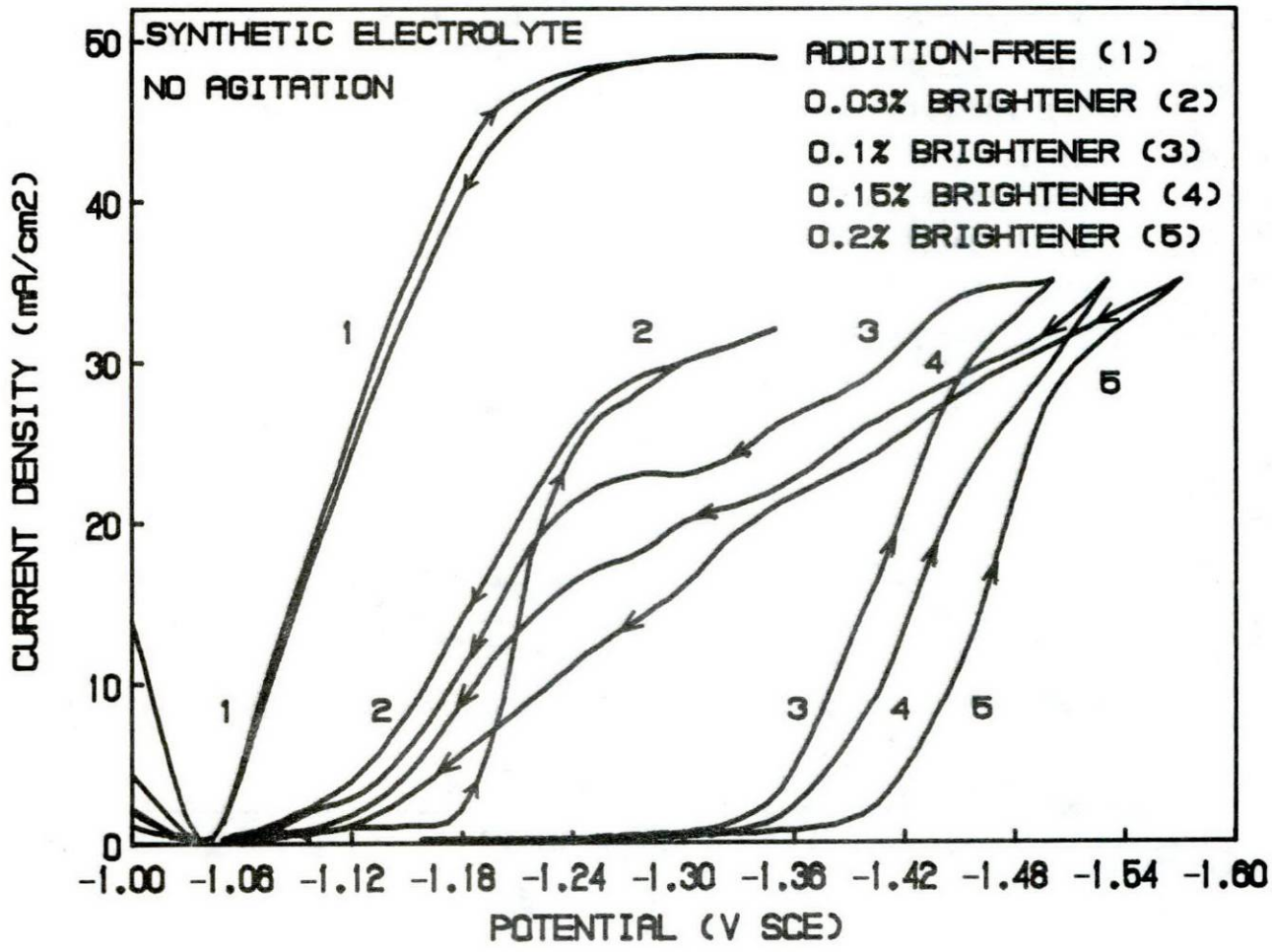

Figure 16. Polarization effects of 1.5% Surfactant III with varying concentrations of commercial brightener in synthetic electrolyte.

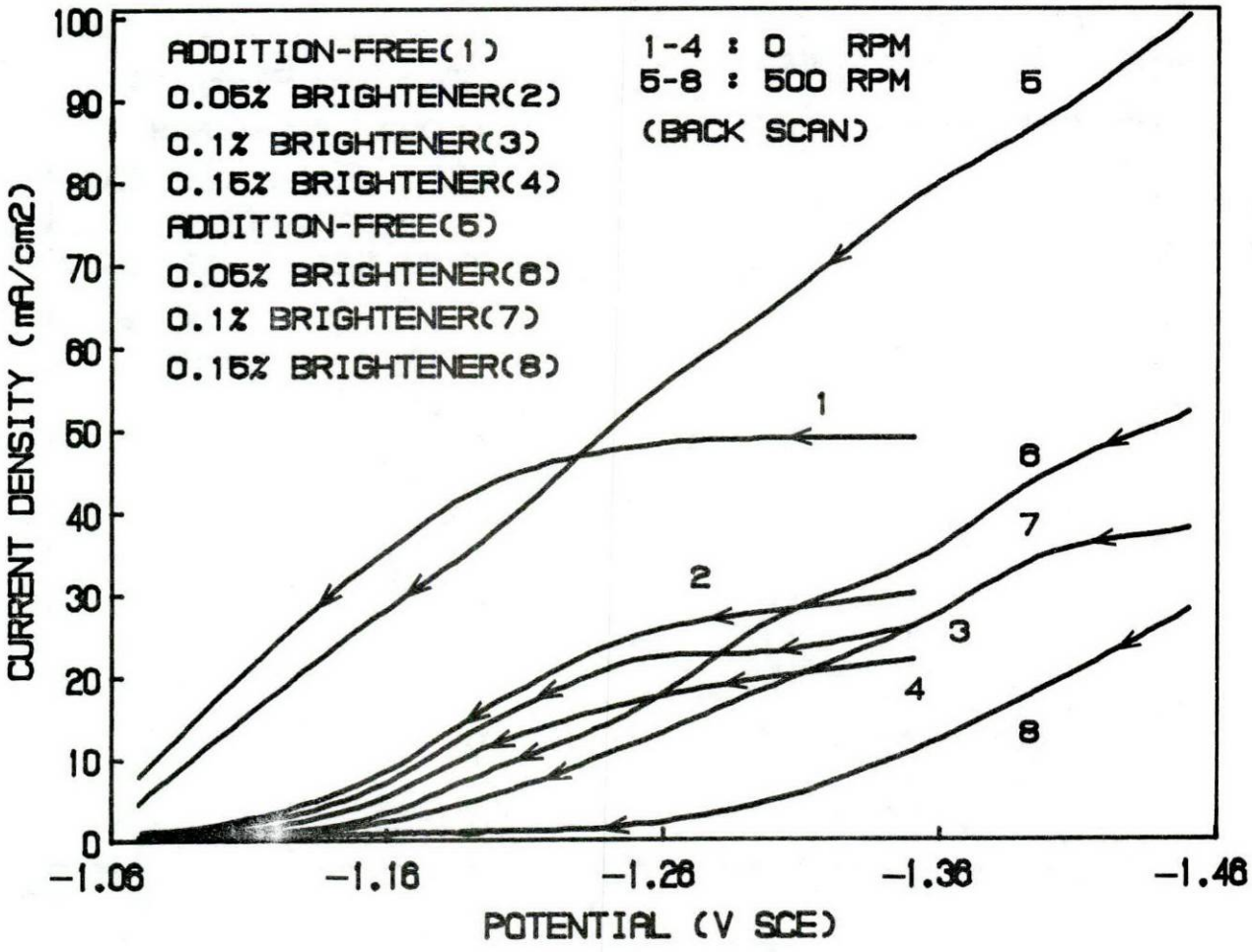

Figure 17. Comparison of polarization effects in the back scan region by 1.5% Surfactant III with varying concentrations of commercial brightener in synthetic electrolyte with and without agitation.

B-6

Research Session B

Addition-Agent Effects in Functional Chromium Deposits

N.M. Martyak
M&T Chemicals, Plating Division
Rahway, NJ 07065

R. Weil
Stevens Institute of Technology
Hoboken, NJ 07030

ADDITION-AGENT EFFECTS IN FUNCTIONAL CHROMIUM DEPOSITS

N. M. Martyak
M&T Chemicals, Plating Division, Rahway, NJ 07065

R. Weil
Stevens Institute of Technology, Hoboken, NJ 07030

INTRODUCTION

Additives are intentionally included in plating solutions for a variety of purposes. They can reduce the grain size by impeding growth. A small grain size is a necessary condition for brightness. A fine grain size is also associated with greater hardness and higher strength. Other additives can result in a better distribution of the grain-refining additive so that growth is inhibited uniformly over the entire deposit surface. Non-uniform growth inhibition leads to crevices which causes loss of brightness, decreased strength and ductility. Addition agents can affect the internal stresses. Exfoliation or cracking of the deposit may be prevented if tensile stresses are decreased or changed to compressive ones. Also, increasing tensile stresses can result in a greater density of the cracks which are characteristic of functional chromium electrodeposits. If additives result in the formation of compounds which are stable at elevated temperatures, they can impede grain-boundary movement and thereby better retain the hardness after annealing.

Brightness, hardness and its retention after heating and the crack patterns which result from internal stress are important properties of chromium electrodeposits. Therefore the effects of certain additives in the plating solution on these properties is of interest and is the topic of this paper.

EXPERIMENTAL PROCEDURES

The compositions of the four plating solutions used in this investigation are listed in Table 1. Chromium from the four plating solutions was deposited at a current density of 0.5A/cm^2 at 55° C on non-hardened steel drill rods. The preplating procedure consisted of degreasing, anodic cleaning in a strong alkaline medium, and anodic etching in the plating solution for 15 sec. The thickness of the deposits from the three additive-containing solutions (i.e., Plating Solutions 2, 3 and 4) was about 100 μm. The thickness obtained from Solution 1 was about 50 μm. Chromium was also deposited on flat steel coupons which were subjected to the same preplating procedure as the drill rods.

Table 1

Composition of Plating Solutions

	Plating Solution 1	Plating Solution 2	Plating Solution 3	Plating Solution 4
CrO_3	2.5M	2.5M	2.5M	2.5M
SO_4^{--}	0.025M	0.014M	0.023M	0.023M
SiF_6^{--}	----	0.025M	----	----
Catalyst A*	----	----	0.543M	0.543M
Additive B(1)	----	----	----	0.001M
Additive C(2)	----	----	----	0.133M

* organo-sulfur compound

Chromium films about 100 nm thick were deposited on electropolished copper foils. The preplating procedure was the same as in a previous investigation(3).

Plated drill rods and flat coupons were annealed in air at 350°, 500° and 850°C for 2 hours. Slices were cut from the as-plated and annealed drill rods and metallographically polished. The hardness of the cross sections of the chromium electrodeposits were measured using a Knoop indenter in a Tukon Hardness Tester and a 100g load. The surfaces of the drill rods were anodically etched in a 2.5M sodium hydroxide solution at 1 A/cm^2 for 1 minute at room temperature in order to develop the crack pattern. The number of cracks per linear cm was determined with an optical microscope. The surfaces of the flat coupons were examined by scanning electron microscopy. The thin chromium films were examined by transmission electron microscopy as previously described(3).

Results and Discussion

The structure of the surfaces of the deposits on the steel coupons, except for the one from the Solution 3 in Table 1, was too fine to resolve by scanning electron microscopy. The sur-

face of the deposit from Solution 3 is shown in Figure 1. Regions surrounded by relatively deep crevices are seen. The surface structure of the deposit from Solution 3 resulted in a matte appearance while that of the other three caused them to be bright. A non-uniform outgrowth from Solution 3 was already apparent in the 100 nm-thick film. Figure 2, which represents the structure of this film, shows some regions which are darker than the rest. Some of these are designated by arrows. The darker regions grew to a greater thickness. It is likely that these faster growing regions also spread laterally. The slower growth between them then resulted in the crevices seen in Figure 1. The thin films from the other three plating solutions exhibited a more uniform outgrowth as can be seen in Figures 3-5. In Figure 3, slightly taller particles can be seen to have grown on a grain boundary in the copper substrate. These particles are also indicated by an arrow. The same phenomenon was observed in the other films, but is not shown in Figues 4 and 5. The extremely fine grain size of all the chromium deposits was resolved by transmission electron microscopy. The smallest, individual black dots, which can be best seen in Figure 5, are the grains. Their size is less than 10 nm.

The likely cause of the crevices seen in Figure 1 is a non-uniform distribution of co-deposited sulfur from Catalyst A. A similar phenomenon was observed by Weil and Jacobus(4) in nickel deposits. When only the sulfur-containing, so-called control agent(5), was present in the plating solution, crevices formed where it was concentrated and preferentially inhibited growth. When the brightener(5) was also present in Solution 4, the deposit was specularly bright as no crevices had formed. Edwards and Levett(6) found that the brightener provides sites where the control agent can adsorb and thus lead to a uniform distribution of the control agent over the surface of the deposit. Apparently, the other additives in Solution 4 acted in a similar manner to cause a uniform inhibition of outgrowth.

The crack densities of the as-plated deposits from the four solutions are listed in Table 2. It is clear that the additives increased the number of cracks compared to the number in the deposit from Solution 1. It is probable that the additives increased the internal tensile stresses. These stresses will be measured and the results should be available when this paper is presented. The larger crack density in the deposit plated from Solution 3 was probably a result of the crevices, which would act as stress raisers.

The hardness values are also listed in Table 2. It is again apparent that the additives increased the hardness. The mechanism of the hardness increase remains to be elucidated.

Table 2

Solution No.	Cracks/cm	Hardness (KHN_{100}) as-plated	350° C	500° C	850° C
1	315	950	700	675	325
2	475	1150	950	875	450
3	700	1300	1450	1500	600
4	475	1400	1450	1525	650

The decrease in hardness on annealing at the temperatures specified can also be seen in Table 2. It appears that the organo-sulfur additive resulted in better hardness retention. A possible cause could be that compounds formed during annealing inhibited the growth of grains. Grain growth typically results in a lower hardness. This phenomenon will also be investigated further.

In summary, it is seen that addition agents can significantly affect the brightness, hardness, retained hardness, and stress in chromium deposits.

REFERENCES

1. M. Perakh, H. Ginsburg, E. Salomon, V. Shargorodsky, and L. Rubinstein, US Patent No. 4,234,396 (1980).

2. N. M. Martyak, US Patent Pending (1988).

3. K. Raghunathan and R. Weil, Surface Technology, 10, 331 (1980).

4. R. Weil and W. N. Jacobus, Jr., Plating, 53, 102 (1966).

5. A. H. DuRose, Trans. Inst. Metal Finish., 38, 27 (1961).

6. J. Edwards and M. J. Levett, ibid, 44, 27 (1966).

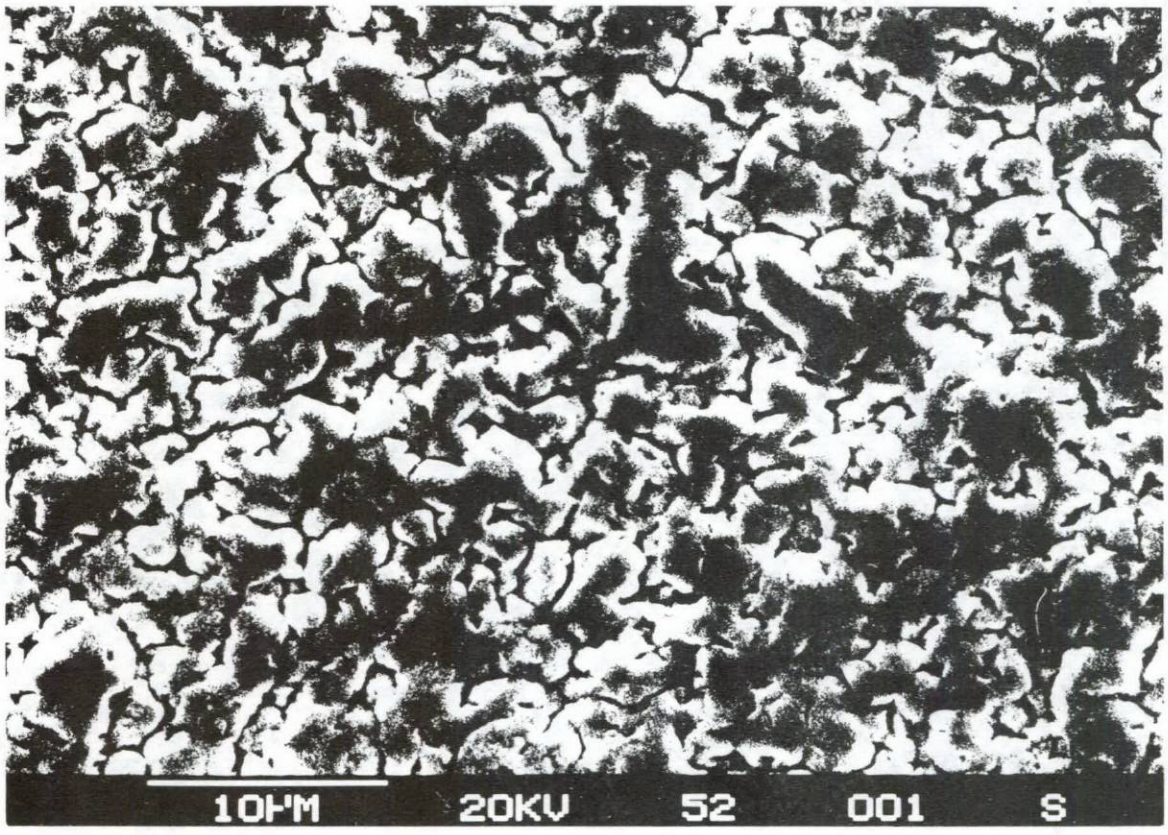

Figure 1. Scanning Electron Micrograph of Deposit from Solution 3

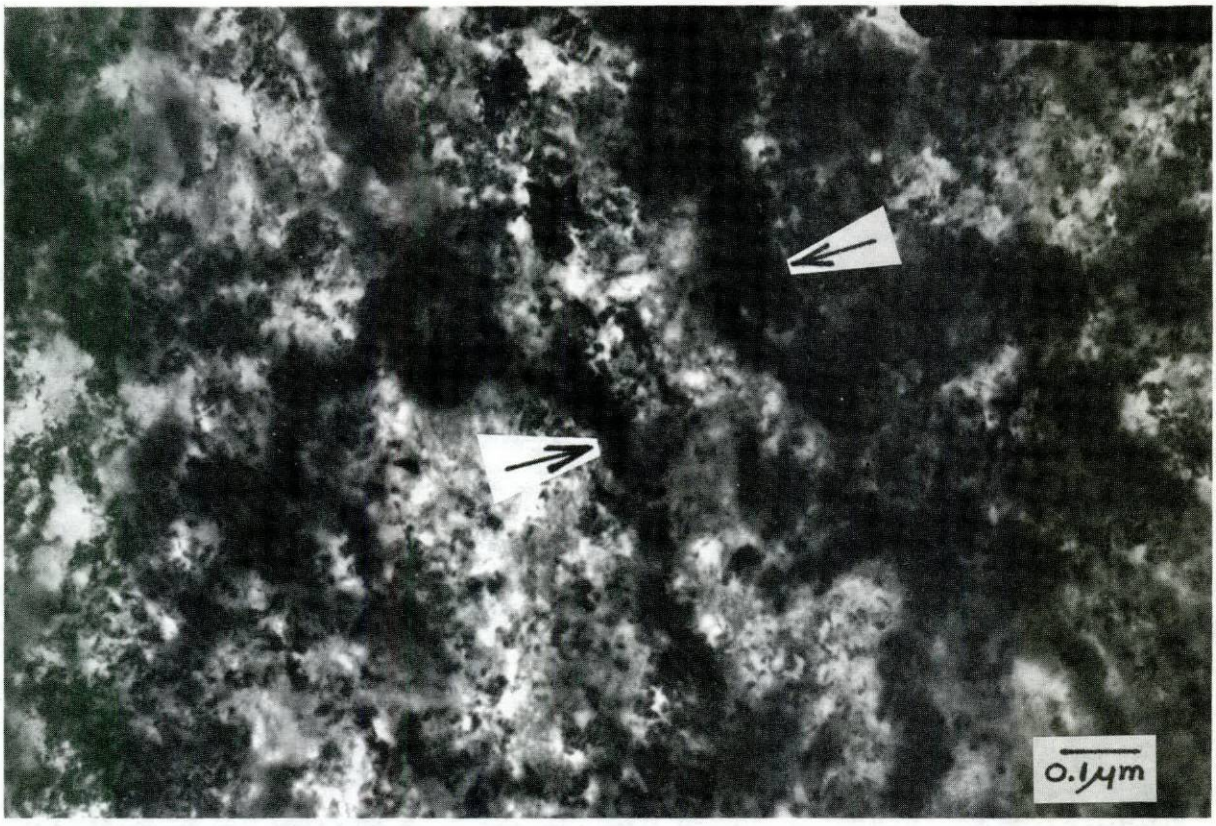

Figure 2. Transmission Electron Micrograph (TEM)
of Deposit from Solution 3.
Arrows indicate faster-growing regions.

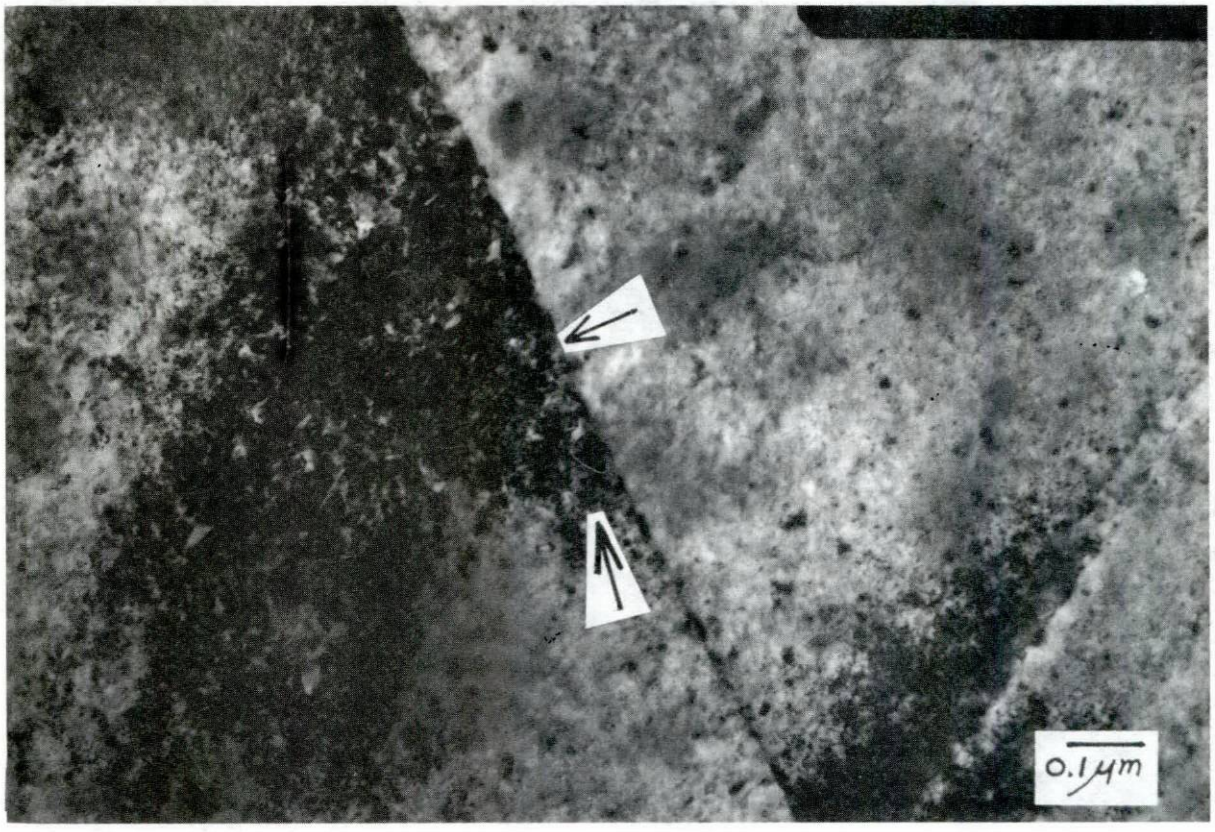

Figure 3. TEM of Deposit from Solution 1. Arrows shows larger particles at substrate grain boundary.

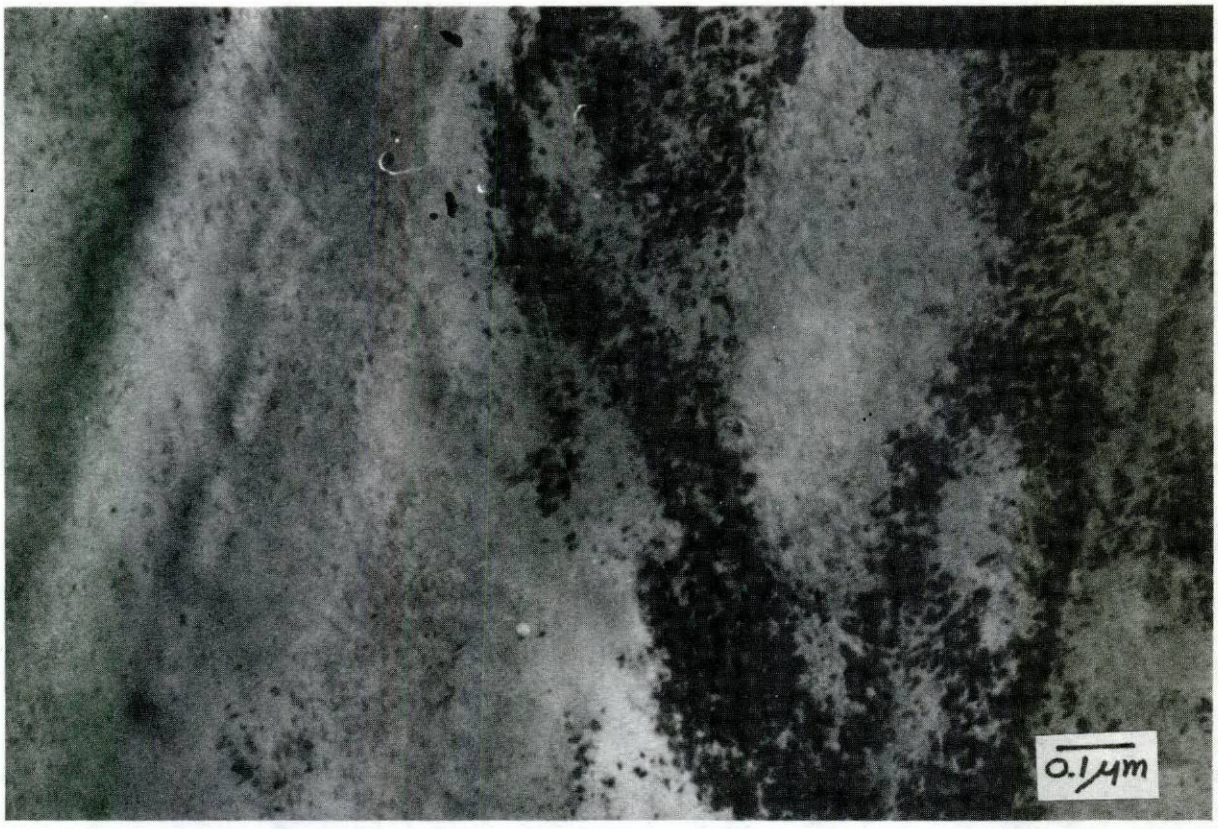

Figure 4. TEM of Deposit from Solution 2.



Figure 5. TEM of Deposit from Solution 4.